

# Global Biogeochemical Cycles®



## RESEARCH ARTICLE

10.1029/2021GB007200

### Key Points:

- Diapycnal mixing and advection and mesoscale eddy stirring supply nutrients to some of the most oligotrophic waters in the North Atlantic
- Diapycnal loss of nutrients below the seasonal boundary layer is partly replenished by eddy stirring in the upper thermocline
- Relay race of nutrient supply by eddy stirring to the upper thermocline passed on by diapycnal mixing and advection to the euphotic zone

### Correspondence to:

R. G. Williams,  
ric@liverpool.ac.uk

### Citation:

Spingys, C. P., Williams, R. G., Tuerena, R. E., Naveira Garabato, A., Vic, C., Forryan, A., & Sharples, J. (2021). Observations of nutrient supply by mesoscale eddy stirring and small-scale turbulence in the oligotrophic North Atlantic. *Global Biogeochemical Cycles*, 35, e2021GB007200. <https://doi.org/10.1029/2021GB007200>

Received 21 SEP 2021  
Accepted 16 NOV 2021




### Author Contributions:

**Conceptualization:** Richard G. Williams  
**Data curation:** Carl P. Spingys, Robyn E. Tuerena  
**Formal analysis:** Carl P. Spingys, Richard G. Williams, Robyn E. Tuerena, Alberto Naveira Garabato, Alexander Forryan  
**Funding acquisition:** Jonathan Sharples  
**Investigation:** Carl P. Spingys, Richard G. Williams, Alberto Naveira Garabato  
**Methodology:** Carl P. Spingys, Richard G. Williams, Robyn E. Tuerena, Alberto Naveira Garabato, Clément Vic, Alexander Forryan  
**Software:** Carl P. Spingys  
**Supervision:** Richard G. Williams  
**Validation:** Carl P. Spingys

© 2021. The Authors.

This is an open access article under the terms of the [Creative Commons Attribution License](https://creativecommons.org/licenses/by/4.0/), which permits use, distribution and reproduction in any medium, provided the original work is properly cited.

## Observations of Nutrient Supply by Mesoscale Eddy Stirring and Small-Scale Turbulence in the Oligotrophic North Atlantic

Carl P. Spingys<sup>1</sup> , Richard G. Williams<sup>2</sup> , Robyn E. Tuerena<sup>3</sup> , Alberto Naveira Garabato<sup>1</sup> , Clément Vic<sup>4</sup>, Alexander Forryan<sup>1</sup>, and Jonathan Sharples<sup>2</sup> 

<sup>1</sup>Ocean and Earth Science, University of Southampton, National Oceanography Centre, Southampton, UK, <sup>2</sup>Department of Earth, Ocean and Ecological Sciences, School of Environmental Sciences, University of Liverpool, Liverpool, UK, <sup>3</sup>Scottish Association for Marine Science, Oban, UK, <sup>4</sup>Laboratoire d'Océanographie Physique et Spatiale, UBO/CNRS/Ifremer/IRD, Plouzané, France

**Abstract** Sustaining biological export over the open ocean requires a physical supply of nutrients to the mixed layer and thermocline. The relative importance of diapycnal mixing, diapycnal advection, and isopycnal stirring by mesoscale eddies in providing this nutrient supply is explored using a field campaign in oligotrophic waters in the subtropical North Atlantic, consisting of transects over and off the mid-Atlantic ridge. Eddy stirring rates are estimated from the excess temperature variance dissipation relative to the turbulent kinetic energy dissipation, and using eddy statistics from satellite observations combined with 9-month-long mooring data. The vertical nutrient fluxes by diapycnal mixing, diapycnal advection, and isopycnal mesoscale eddy stirring are assessed using nitrate measurements from observations or a climatology. Diapycnal mixing and advection provide a nutrient supply within the euphotic zone, but a loss of nutrients within the upper thermocline. Eddy stirring augments, and is comparable to, the diapycnal transfer of nutrients within the summertime upper thermocline, while also acting to replenish nutrients within the deeper parts of the thermocline. The eddy supply of nitrate is relatively small in the center of the subtropical gyre, reaching up to  $0.06 \text{ mol N m}^{-2}\text{yr}^{-1}$ , but is likely to be enhanced on the flanks of the gyre due to larger isopycnal slopes and lateral nitrate gradients. The nutrient supply to the euphotic zone is achieved via a multistage mechanism: a diapycnal transfer of nutrients by small-scale turbulence to the euphotic zone, and an isopycnal stirring of nutrients by mesoscale eddies replenishing nutrients in the upper thermocline.

**Plain Language Summary** Phytoplankton growth requires a supply of nutrients to the base of the euphotic zone, which is usually provided by a combination of vertical mixing or vertical upwelling of nutrients. However, in the oligotrophic waters of the central North Atlantic, it is unclear how the vertical supply of nutrients is sustained. Here, we use field data to explore the roles of mixing across density surfaces, advection across density surfaces and mesoscale eddy stirring along density surfaces in supplying nutrients to some of the most nutrient-depleted surface waters in the central North Atlantic. Diapycnal mixing and advection are found to be important in supplying nutrients to the euphotic zone during summer, but at the expense of eroding the nutrients in the upper thermocline. In contrast, mesoscale eddy stirring augments the diapycnal supply of nutrients to the euphotic zone and replenishes nutrients in the upper thermocline.

## 1. Introduction

Biological export of organic matter in the open ocean is usually viewed as being sustained by a vertical supply of nutrients to the euphotic zone from the upper thermocline. This vertical transfer of nutrients is easily provided in regions of climatological wind-driven upwelling, but is more difficult to achieve in downwelling areas, where a combination of diapycnal transfer and time-dependent upwelling needs to take place.

Maintaining biological export is particularly challenging in the oligotrophic waters of the North Atlantic subtropical gyre, where tracer-based estimates of export production range from  $0.42$  to  $0.65 \text{ mol N}^{-2}\text{m}^{-2}\text{y}^{-1}$  in the Sargasso Sea (Jenkins & Goldman, 1985; Jenkins, 1988; Jenkins & Wallace, 1992; Stanley et al., 2015). These estimates of export production are at least twice as large as those based on conventional estimates of nitrate supply, combining together the contributions from atmospheric deposition (Knap et al., 1986), convective entrainment (Michaels et al., 1994), diapycnal mixing (Lewis et al., 1986; Dietze et al., 2004), and horizontal Ekman transfers (Williams & Follows, 1998).

**Writing – original draft:** Carl P. Spingys, Richard G. Williams  
**Writing – review & editing:** Carl P. Spingys, Richard G. Williams, Robyn E. Tuerena, Alberto Naveira Garabato, Jonathan Sharples

Time-varying circulations involving mesoscale eddies and fronts have been invoked to partly explain the mismatch between estimates of nutrient supply and export (McGillicuddy Jr & Robinson, 1997; McGillicuddy et al., 1998; Lévy et al., 2001). Such mesoscale circulations may affect both vertical and horizontal transfers of nutrients (Lee & Williams, 2000; Williams & Follows, 2003; Resplandy et al., 2011; Lévy et al., 2012). In particular, time-varying eddy flows have been argued to provide a rectified pumping of nutrients into the euphotic zone: an upward intrusion of nutrients into the euphotic zone leads to biological consumption, while a downward intrusion of nutrients into the dark ocean interior leads to no biological response (McGillicuddy Jr & Robinson, 1997). While this rectification process is appealing in potentially sustaining an enhanced nutrient supply to the euphotic zone, there is a price that remains unresolved from this process: an underlying loss of nutrients from the thermocline.

This difficulty in sustaining nutrient levels in the upper thermocline is highlighted in two contrasting model experiments. McGillicuddy Jr et al. (2003) illustrated how time-varying eddies may provide a dominant supply of nitrate to the euphotic zone over the subtropical gyre, overcoming the effects of large-scale wind-driven downwelling, in an eddy-resolving model study including an artificial restoring of nutrients below the euphotic zone. In contrast, Oschlies (2002) found a much weaker eddy supply of nutrients to the euphotic zone in model integrations without this interior restoring. Thus, the maintenance of the nutrient concentrations in the thermocline is central to whether time-varying, vertical motions may account for a sustained nutrient supply to the euphotic zone.

In our work, the question of how nutrients in the thermocline are sustained against the action of processes supplying nutrients to the overlying euphotic zone is explored in terms of the competing effects of nutrient transfers by small-scale mixing across density surfaces, referred to as diapycnal mixing, advection across density surfaces, referred to as diapycnal advection, and mesoscale eddy stirring along density surfaces, referred to as isopycnal stirring. First, a theoretical context is provided for how the nutrient budget for a density layer is affected by advective and diffusive nitrate fluxes, including diapycnal transfers from microstructure and the isopycnal effects of mesoscale eddy advection and diffusion (Section 2). Then, observations from a summer field campaign conducted in some of the most oligotrophic waters of the subtropical North Atlantic, in the vicinity of the Mid-Atlantic Ridge (Tuerena et al., 2019), are considered (Section 3) to estimate the rates of diapycnal mixing, diapycnal advection, and isopycnal stirring by mesoscale eddies (Section 4). The supply of nutrients by diapycnal mixing, diapycnal advection, and isopycnal stirring is then assessed, for different density classes, along two transects over and off the Mid-Atlantic Ridge (Section 5). The relevance of our findings is then discussed for our field site and for the rest of the North Atlantic subtropical gyre (Section 6).

## 2. Theoretical Context

Our aim is to focus on the transfers of nutrients by both microscale turbulence and by mesoscale eddies using an isopycnal formulation. The layer-integrated tracer equation is firstly discussed for a nutrient, then the relevant diffusive transfer terms identified, and closures applied to estimate these terms.

### 2.1. Thickness-Weighted Tracer Equation

Following Bleck and Boudra (1981), Bleck (1998), and McDougall (1984), the tracer equation integrated over the thickness of the density layer may be written as

$$\underbrace{\frac{\partial}{\partial t}(hN)}_{\text{tendency}} + \underbrace{\nabla_{\sigma} \cdot (h\mathbf{u}N)}_{\text{isopycnal advection}} + \underbrace{(w^*N)|_{\text{bot}} - (w^*N)|_{\text{top}}}_{\text{diapycnal advection}} = \underbrace{\nabla_{\sigma} \cdot (\nu h \nabla_{\sigma} N)}_{\text{isopycnal diffusion}} + \underbrace{F_{\text{dia}}|_{\text{bot}} - F_{\text{dia}}|_{\text{top}}}_{\text{diapycnal diffusion}} + \underbrace{hS}_{\text{biological source}}, \quad (1)$$

where  $h$  is the vertical thickness of the isopycnal layer,  $N$  is the nutrient tracer,  $\mathbf{u}$  is the velocity along the density layer,  $\nabla_{\sigma}$  is the gradient along a density surface,  $w^*$  is the diapycnal velocity across the bounding density surfaces, denoted bottom and top,  $\nu$  is the isopycnal diffusivity from microscale turbulence,  $F_{\text{dia}}$  is the diapycnal tracer flux across the bounding density surfaces, and  $S$  is the biological source. The gradient  $\nabla_{\sigma}$  is evaluated with the distance taken from a projection along a horizontal plane, which avoids the inclusion of metric terms (Bleck & Boudra, 1981).

The diapycnal velocity,  $w^*$ , follows the notation of McDougall (1984) and is equivalent to  $\delta z/\delta\sigma$  in the notation of Bleck and Boudra (1981). The diffusive and diapycnal transfers are all taken to be representative of microscale turbulence.

Following Gent et al. (1995), consider the effect of time-varying mesoscale eddies, which is assumed to act to transfer tracers along density surfaces. Take a prime to represent a mesoscale eddy deviation and an overbar to represent a time average over the lifetime of many mesoscale eddy events, so that all variables are separated into mean and mesoscale eddy contributions, such as  $\mathbf{u} = \bar{\mathbf{u}} + \mathbf{u}'$ . Applying this partitioning to the thickness-weighted flux of tracer along the density layer,  $h\mathbf{u}N$ , and then applying a time average over the lifetime of many mesoscale eddies, obtains

$$\underbrace{\overline{h\mathbf{u}N}}_{\text{isopycnal tracer flux}} = \underbrace{\overline{(h\bar{\mathbf{u}} + h'\mathbf{u}')N}}_{\text{advective tracer flux}} + \underbrace{\overline{(h\mathbf{u}')N'}}_{\text{diffusive tracer flux}}, \quad (2)$$

where (i) the time-mean tracer  $\bar{N}$  is advected along the density layer by the time-mean velocity  $\bar{\mathbf{u}}$  and the time-varying mesoscale eddies,  $h'\mathbf{u}'/\bar{h}$ , involving a correlation in velocity and layer thickness, and (ii) the tracer is diffused along the density layer by the mesoscale eddy correlations in the volume flux,  $(h\mathbf{u})'$ , and tracer concentration,  $N'$ .

Combining (1) and (2), the tracer equation integrated over a density layer and including a time average over the lifetime of eddy events is given by

$$\underbrace{\frac{\partial}{\partial t}(\overline{hN})}_{\text{tendency}} + \underbrace{\nabla_{\sigma} \cdot ((h\bar{\mathbf{u}} + h'\mathbf{u}')N)}_{\text{isopycnal advection}} + \underbrace{(\overline{w^*N})|_{bot} - (\overline{w^*N})|_{top}}_{\text{diapycnal advection}} = \underbrace{-\nabla_{\sigma} \cdot (\overline{(h\mathbf{u}')N'}) + \nabla_{\sigma} \cdot (v\overline{h\nabla_{\sigma}N})}_{\text{isopycnal diffusion}} + \underbrace{\overline{F_{dia}}|_{bot} - \overline{F_{dia}}|_{top}}_{\text{diapycnal diffusion}} + \underbrace{\overline{hS}}_{\text{biological source}}, \quad (3)$$

The evolution of the nutrient in the layer is then determined by (i) the isopycnal advection by the time-mean flow and the mesoscale eddies; (ii) the diapycnal advection of the tracer across the bounding density surfaces; (iii) an isopycnal diffusive transfer by a combination of mesoscale eddies and microscale turbulence; (iv) a diapycnal diffusion by microscale turbulence; and (v) a biological source including a rectification by eddy changes in layer thickness.

The mesoscale and microscale turbulent processes affect the tracer balance in distinct ways. The microscale turbulence provides a diapycnal diffusion and isopycnal diffusion of tracer together with a diapycnal advection of tracer (McDougall, 1984; McDougall, 1987; Groeskamp, Griffies, et al., 2019). Mesoscale eddies provide an isopycnal transfer of tracer, involving both an isopycnal advection defining a bolus velocity given by  $h'\mathbf{u}'/\bar{h}$ , and an isopycnal diffusion given by  $(h\mathbf{u}')N'$ . There may also be an additional eddy advection of the tracer due to a skew flux contribution linked to the tracer distribution (Canuto & Dubovikov, 2011), which we ignore here. These isopycnal advective and diffusive effects of mesoscale eddies have distinctive tracer signals (Lee et al., 1997) and are parameterized separately in ocean models (Gent & McWilliams, 1990; Redi, 1982).

## 2.2. Diffusive Nutrient Supply

Using field data, we wish to compare the magnitude of the different nutrient supply terms within the seasonal boundary layer and thermocline in the tracer equation (3) involving the convergences of the diapycnal diffusion by microstructure, the diapycnal advection by microstructure, and the isopycnal diffusion by mesoscale eddies over an isopycnal layer of thickness  $h$ , which are represented, respectively, by

$$\underbrace{(\overline{F_{dia}}|_{bot} - \overline{F_{dia}}|_{top})/\bar{h}}_{\text{diapycnal diffusion}}, \quad \underbrace{((\overline{w^*N})|_{bot} - (\overline{w^*N})|_{top})/\bar{h}}_{\text{diapycnal advection}} \quad \text{and} \quad \underbrace{-(1/\bar{h})\nabla_{\sigma} \cdot \overline{(h\mathbf{u}')N'}}_{\text{isopycnal diffusion}},$$

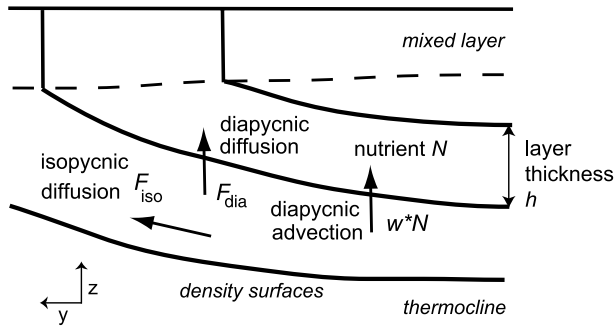


**Figure 1.** The diffusive nutrient flux,  $\mathbf{F}$ , may be separated into diapycnal and isopycnal components for a density layer with a nutrient concentration  $N$  and layer thickness  $h$ , the diffusive nutrient flux,  $\mathbf{F}$ , may be viewed as the sum of a diapycnal component directed across density surfaces (driven by microscale turbulence),  $F_{dia}$ , and an isopycnal component induced by mesoscale eddy stirring,  $F_{iso}$ . Diapycnal advection,  $w^*$ , is formed by contrasts in the diapycnal diffusive flux of density and is directed towards regions of turbulence, and so also provides a diapycnal nutrient flux,  $w^*N$ . The diapycnal and isopycnal transfers are potential mechanisms to supply nutrients,  $N$ , to the upper thermocline and mixed layer, and so contribute to sustaining export production from the euphotic zone.

which are in units of  $\text{mol N m}^{-3}\text{s}^{-1}$  (Figure 1). The isopycnal diffusion from mesoscale eddies is much larger than the contribution from microscale turbulence (Tennekes & Lumley, 2018), so the microscale turbulence contribution is ignored here.

### 2.2.1. Closure for Diapycnal Diffusion

The diapycnal diffusive flux of nutrients associated with microscale turbulence is parameterized here by a down-gradient closure,

$$\overline{F}_{dia} = -\kappa_{dia} \frac{\partial \overline{N}}{\partial z}, \quad (4)$$

where  $\kappa_{dia}$  is a diapycnal diffusivity. Hence, the convergences in the diapycnal diffusive tracer fluxes in (3) may be reexpressed as

$$\frac{\overline{F}_{dia}|_{bot} - \overline{F}_{dia}|_{top}}{\overline{h}} = \frac{1}{\overline{h}} \left( - \left( \kappa_{dia} \frac{\partial \overline{N}}{\partial z} \right) \Big|_{bot} + \left( \kappa_{dia} \frac{\partial \overline{N}}{\partial z} \right) \Big|_{top} \right). \quad (5)$$

### 2.2.2. Closure for Diapycnal Advection

Diapycnal advection is generated by contrasts in the diapycnal diffusive density flux. The diapycnal velocity,  $w^*$ , is defined here by

$$w^* = \frac{\partial F_{dia,\gamma}}{\partial \gamma} = \frac{\partial}{\partial \gamma} \left( -\kappa_{dia} \frac{\partial \gamma}{\partial z} \right), \quad (6)$$

where  $F_{dia,\gamma}$  is the diapycnal diffusive flux of density,  $\gamma$  is the neutral density, and  $\kappa_{dia}$  is the diapycnal diffusivity (Nurser et al., 1999; de Lavergne et al., 2016). The diapycnal velocity is directed towards the regions of enhanced mixing. Here, we define the diapycnal velocity as positive towards lighter classes due to our focus on upward nutrient fluxes towards the euphotic zone, even though previous studies often define it as positive towards denser classes. This closure excludes the effective advection driven by the nonlinearity of the equation of state, however, this effect is typically small at low- and midlatitudes (Klocker & McDougall, 2010).

The diapycnal advection of nitrate is found to be important on annual time scales when integrated over the entire water column (Groeskamp, Griffies, et al., 2019), although it is unclear how important this diapycnal advection of nitrate is within the thermocline.

### 2.2.3. Closure for Isopycnal Diffusion by Mesoscale Eddies

The isopycnal diffusive transfer of nutrients is viewed here as being provided by mesoscale eddies, involving quasi-geostrophic circulations stirring nutrients along density surfaces in an adiabatic manner. The thickness-weighted diffusive flux of nutrients,  $(\overline{hu})'N'$ , is assumed to be mainly determined by the eddy correlations in velocity and nutrient concentration, such that  $(\overline{hu})'N' \simeq \overline{h} \overline{\mathbf{u}'N'}$ , which is parameterized in terms of the isopycnal gradient in nutrients, so that the isopycnal flux of nutrients,  $\overline{\mathbf{F}}_{iso}$ , is given by

$$\overline{\mathbf{F}}_{iso} = \overline{(\overline{hu})'N'} / \overline{h} = -\kappa_{iso} \nabla_{\sigma} \overline{N}, \quad (7)$$

where  $\kappa_{iso}$  is an isopycnal diffusivity and  $\nabla_{\sigma}$  denotes the gradient along density surfaces. Hence, the convergences in the isopycnal diffusive tracer flux from mesoscale eddies in (3) may be reexpressed as

$$-\nabla_{\sigma} \cdot \overline{(\overline{hu})'N'} = -\nabla_{\sigma} \cdot (\overline{h} \overline{\mathbf{F}}_{iso}) = \nabla_{\sigma} \cdot (\overline{h} \kappa_{iso} \nabla_{\sigma} \overline{N}). \quad (8)$$

The convergence in the diffusive isopycnal flux of nutrients in (8) can be rewritten using a coordinate transformation where the isopycnal gradient is made up of the sum of a horizontal gradient at a constant depth and the isopycnal slope multiplied by a vertical gradient at the density surface,

$$\nabla_{\sigma} \cdot \overline{(\overline{hu})'N'} = \nabla_z \cdot \overline{(\overline{hu})'N'} + \mathbf{S} \cdot \frac{\partial}{\partial z} \overline{(\overline{hu})'N'} \quad (9)$$

where  $\nabla_z$  is the horizontal gradient operator and the vector representing the isopycnal slope is given by  $\mathbf{S} = \mathbf{i}\partial z/\partial x|_\sigma + \mathbf{j}\partial z/\partial y|_\sigma$  with  $\mathbf{i}$  and  $\mathbf{j}$  unit vectors in the  $x$  and  $y$  directions.

Next, we apply this theoretical framework to field observations to assess the relative roles in sustaining nutrients in the upper thermocline of the North Atlantic subtropical gyre from the diapycnal diffusive nutrient supply from microscale turbulence in (5), the diapycnal advective nutrient supply from microscale turbulence (6), and the isopycnal diffusive nutrient supply from mesoscale eddies in (8).

### 3. Field Program

The observations analyzed here were obtained by a field study in some of the most oligotrophic waters of the North Atlantic subtropical gyre, between 24°N to 36°N, as part of the RidgeMix program to investigate the role of internal tides in diapycnal nutrient supply to the euphotic zone (Figure 2a). The sampling campaign was conducted on the *RRS James Clark Ross* (cruise JR15007) in May to June 2016. The field program involved 67 stations sited either along the crest of the Mid-Atlantic Ridge or in the adjacent deep-ocean basin (Figure 2a, blue and red dots, respectively). There is a marked difference in the intensity of small-scale turbulence and associated nutrient fluxes between the on- and off-ridge regions (Tuerena et al., 2019), so that our subsequent analyses are accordingly separated into on- and off-ridge areas.

At all of the CTD stations, temperature, salinity, and water samples were measured for the full depth or the upper 1000 m of the water column. Micro-molar nutrient measurement was carried out at all CTD stations, for the analysis of nitrate, nitrite, phosphate, and silicate, using a four-channel Bran and Luebbe AAIH segmented flow, colorimetric, autoanalyzer. Two internal standards for nitrate, phosphate, and silicate were analyzed in each run, covering the range of concentrations in the deep and surface layers. Certified reference materials (Kanso) were analyzed every 2-3 runs to ensure continued precision throughout the cruise, and cruise averages within the accepted range for each nutrient and with a 99% precision.

In this region, the mixed layer extends to a depth of less than 50 m during summer, and increases to respective depths of 150 m to 100 m at the end of winter at 36°N and 24°N, based upon climatology (Figures 2b and 2c, red and blue dashed lines). The density surfaces, strictly Neutral Density (Jackett & McDougall, 1997), outcropping in the winter mixed layer over the region include  $\gamma = 26$  to 26.5 ( $\text{kg m}^{-3}$ ). The cruise sections reveal the expected southward deepening of density surfaces within the subtropical gyre (Figure 2c, black lines). The euphotic zone ranges from depths of 50 m to 150 m, and contains waters that are relatively depleted in nitrate (Figure 2c, dashed magenta line and green dots). Below the euphotic zone, there are relatively enriched nutrients, reaching typically 5  $\mu\text{mol kg}^{-1}$  at 250 m both along and off the ridge (Figure 2c, green dots). The deep chlorophyll maximum deepens southward from a depth of 150 m at 36°N to 200 m at 26°N (Figure 2c, dashed magenta line and blue shading).

Measurements of microstructure temperature variance and velocity shear were made at 30 of the stations using a free-falling Vertical Microstructure Profiler (VMP-6000, Rockland Scientific). The microstructure was measured on the length scales of dissipation of turbulent flows, typically a few millimeters to tens of centimeters. The rates of dissipation of turbulent kinetic energy,  $\epsilon$  ( $\text{W kg}^{-1}$ ), and of temperature variance,  $\chi$  ( $^{\circ}\text{C}^2\text{s}^{-1}$ ), were estimated following the standard methods after Oakey (1982).

A mooring provided measurements of horizontal velocity for the full water column for 9 months between September 2015 and July 2016 at 36.23°N, 32.75°W (Figure 2a). The mooring included two Teledyne RD Instruments 75-kHz Long Ranger acoustic Doppler current profilers (ADCPs) and two Flowquest 75-kHz ADCPs. All ADCPs recorded hourly-averaged horizontal velocity in 8 m vertical bins (Vic et al., 2018).

### 4. Estimating Diapycnal Mixing, Diapycnal Advection, and Isopycnal Eddy Stirring From Observational Data

The rates of diapycnal mixing and advection by small-scale turbulence and isopycnal stirring by mesoscale eddies are now assessed using the field observations. Although the diapycnal diffusivity associated with small-scale turbulence is typically 8 orders of magnitude smaller than the isopycnal diffusivity linked to mesoscale eddy stirring, the nutrient gradient across density surfaces is much greater than the nutrient gradient along density surfaces, such that diapycnal and isopycnal diffusive fluxes of nutrients are broadly comparable in magnitude.

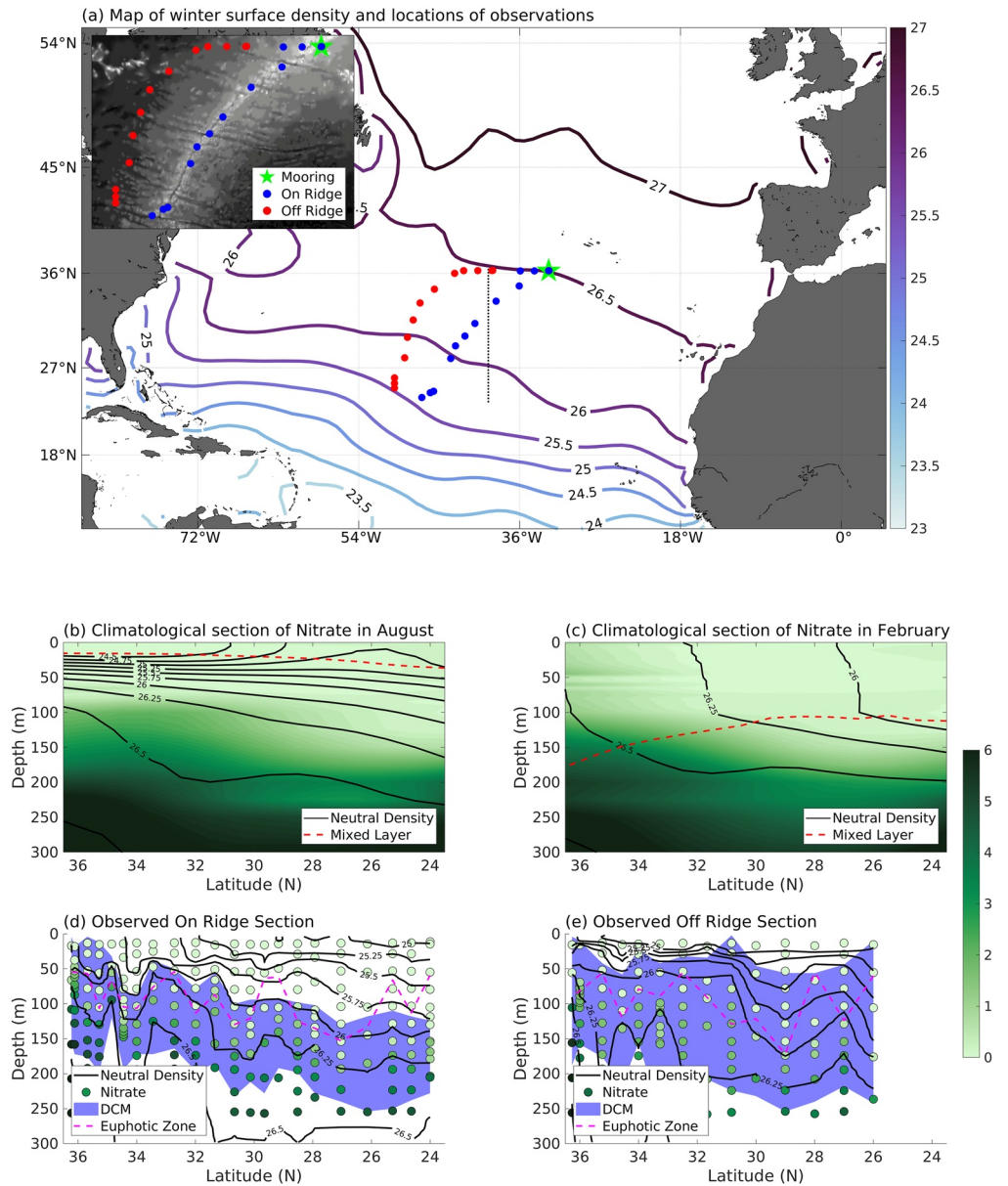


**Figure 2.** Context of the observational study showing: (a) map of the February surface density from climatology, with the locations of: stations marked with circles, separated into on-ridge (blue) and off-ridge (red); the mooring (green star); and the location of climatology sections (grey lines). The inset shows the positions of the observations against the backdrop of topography. Climatological meridional sections for (b) August and (c) February for nitrate ( $\mu\text{mol kg}^{-1}$ , background colors), neutral density (black lines), and the base of the mixed layer (red dashed line). Observed meridional sections for (d) on-ridge or (e) off-ridge, showing nitrate (green circles), neutral density (black lines), deep chlorophyll maximum (DCM, blue shading), and the base of the euphotic zone (dashed magenta line). The DCM is defined by the depth of a 10% variation in the maximum fluorescence, and the base of the euphotic zone is defined by 1% of photosynthetic radiation measured at a depth of 6 m.

#### 4.1. Diapycnal Diffusivity

The diapycnal diffusivity associated with small-scale turbulence is diagnosed using a turbulence closure (Osborn, 1980), which assumes a balance between the rates of turbulent kinetic energy dissipation and the turbulent buoyancy flux,

$$\kappa_{dia} = \Gamma \frac{\epsilon}{N^2}, \quad (10)$$

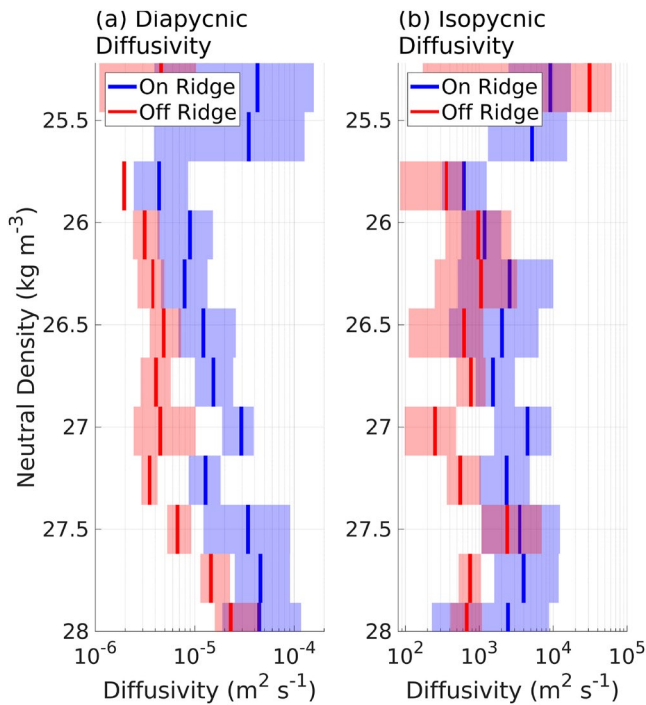


**Figure 3.** Profiles in neutral density of (a) the average diapycnal diffusivity and (b) the average isopycnal diffusivity for the on-ridge (blue) and off-ridge (red) stations. Shading indicates the 95% bootstrap confidence interval.

where,  $\Gamma$  is the dissipation ratio indicating the proportion of the turbulent kinetic energy being used to mix tracers,  $N^2$  is the buoyancy frequency defined as  $N^2 = -\frac{g}{\rho} \frac{\partial \sigma}{\partial z}$  (where  $\sigma$  is the local potential density and  $g$  is the gravitational acceleration), and the empirical choice of  $\Gamma = 0.2$  is representative for stratified shear turbulence (Gregg et al., 2018). The diapycnal diffusivity,  $\kappa_{dia}$ , is diagnosed in neutral density bins of  $0.12 \text{ kg m}^{-3}$  calculated using the routines of Jackett and McDougall (1997).

The diapycnal diffusivity is systematically enhanced over the Mid-Atlantic Ridge relative to off the ridge by a factor of typically 2 to 6, ranging from  $5 \times 10^{-5} \text{ m}^2 \text{ s}^{-1}$  to  $4 \times 10^{-6} \text{ m}^2 \text{ s}^{-1}$  for neutral surfaces between  $\gamma = 25.5$  and 28 (Figure 3a, blue and red lines). In both cases these diffusivities are much larger than molecular diffusivity, typically  $10^{-7} \text{ m}^2 \text{ s}^{-1}$ , implying the diffusivity can reasonably be applied to any tracer.

#### 4.2. Diapycnal Advection

The diapycnal advection,  $w^*$ , is generated by a convergence in the diapycnal diffusive density flux,  $F_{dia,\gamma}$  from equation (6). The diapycnal diffusivity is larger on the lighter and denser surfaces with a minimum at  $\gamma = 26.2$ , and the vertical gradient in the neutral density is larger for density layers lighter than  $\gamma = 26.2$ , but relatively weak for denser layers (Figures 4a and 4b). The resulting diapycnal diffusive density flux,  $F_{dia,\gamma}$ , is directed towards denser surfaces, with larger values along lighter surfaces and a minimum value close to  $\gamma = 26.4$  (Figure 4c). The diapycnal advection,  $w^*$ , is then directed towards the regions of elevated turbulence, i.e. from dense to light surfaces for densities lighter than  $\gamma = 26.4$ , but towards larger densities from  $\gamma = 27$  (Figure 4d). There is the same vertical structure for the diapycnal advection

both on and off ridge, although  $w^*$  is typically an order of magnitude higher on the ridge due to the stronger tidal mixing. The errors in the estimate of  $w^*$  are large due to taking the diapycnal gradient of the diapycnal diffusivity, which has large uncertainties, combined with the vertical gradient of neutral density.

Hence, this structure of the diapycnal velocity,  $w^*$ , directed towards the density extremes, is consistent with the most intense turbulence in the water column occurring near the surface and bottom boundaries, most likely driven by wind forcing and flow-topography interaction, and a mid-water column minimum. Such vertical structure in the intensity of turbulent mixing and resultant diapycnal velocities is compatible with previous observations on a global scale (Kunze et al., 2006; Waterhouse et al., 2014).

#### 4.3. Isopycnal Diffusivity From a Tracer Variance Approach

The isopycnal diffusivity associated with mesoscale eddy stirring is diagnosed using a temperature variance budget approach (Ferrari & Polzin, 2005),

$$\underbrace{\frac{\partial \overline{\theta'^2}}{\partial t}}_{\text{tendency}} + \underbrace{\nabla \cdot (\overline{\mathbf{u}\theta'^2} + \overline{\mathbf{u}'\theta'^2} - \kappa_\theta \nabla \overline{\theta'^2})}_{\text{advective and diffusive fluxes}} + \underbrace{2\overline{\mathbf{u}'\theta'}}_{\text{production}} \cdot \nabla \overline{\theta} = \underbrace{-\chi}_{\text{dissipation}}, \quad (11)$$

where  $\theta$  is the potential temperature,  $\chi$  is the rate of dissipation of temperature variance,  $\kappa_\theta$  is the molecular diffusivity of temperature, the velocity is a full three-dimensional velocity, and  $\nabla$  is a full three-dimensional gradient operator here, and again the overbar indicates a time average over many eddy events and the primes indicate the deviation from this average. There is a balance between the tendency of temperature variance, the divergence of the advective and diffusive fluxes of variance, production of temperature variance, and the dissipation of temperature variance.

In our observations, the root mean square temperature anomalies on density surfaces are  $\overline{\theta'^2} = 0.1 \text{ }^\circ\text{C}$  at depth, increasing to  $0.3 \text{ }^\circ\text{C}$  towards the surface. By combining these estimates with temperature variance dissipation rates,

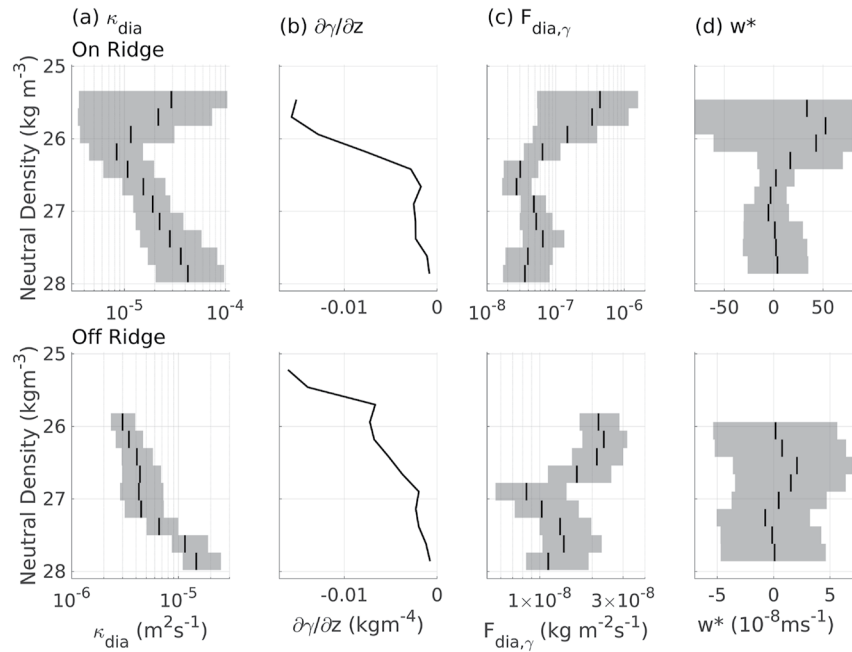


**Figure 4.** The diapycnal advection for the on-ridge (upper row) and off-ridge (lower row) stations. The profiles: (a) diapycnal diffusivity,  $\kappa_{dia}$  ( $\text{m}^2\text{s}^{-1}$ ), (b) vertical density gradient,  $\partial\gamma/\partial z$  ( $\text{kg m}^{-4}$ ), (c) the diapycnal diffusive flux of density,  $F_{dia,\gamma}$  ( $\text{kg m}^{-2}\text{s}^{-1}$ ), positive directed towards denser surfaces, and (d) diapycnal advection,  $w^*$  ( $\text{m s}^{-1}$ ), positive directed upwards. The black lines show the mean values derived from the microstructure data and the cruise-observed gradients. The shaded regions indicate 95% confidence ranges using a bootstrap method.

typically  $\chi = 10^{-9} \text{ }^\circ\text{C}^2\text{s}^{-1}$  at depth to  $10^{-8} \text{ }^\circ\text{C}^2\text{s}^{-1}$  near the surface, then a lifetime for the temperature variance can be estimated of typically 100 days (see Naveira Garabato et al. (2016)). Assuming a background mean flow for this region of  $0.01 \text{ ms}^{-1}$ , then the temperature variance is likely to be advected over a horizontal scale of 100 km before being dissipated, which is a much smaller scale than the horizontal extent of our sections spanning 1000 to 2000 km. Hence, the tendency, advection, and diffusion terms in (11) are neglected, so that an approximate local balance is assumed to hold between the production and dissipation of temperature variance,

$$\overline{\mathbf{u}'\theta'} \cdot \nabla \bar{\theta} = -\chi/2. \quad (12)$$

Following Naveira Garabato et al. (2016), the production of temperature variance is decomposed into (i) microscale turbulence providing a diapycnal transfer and (ii) mesoscale eddy stirring providing an isopycnal transfer:

$$\overline{\mathbf{u}'_t\theta'_t} \cdot \frac{\partial \bar{\theta}}{\partial z} + \overline{\mathbf{u}'_e\theta'_e} \cdot \nabla_\sigma \bar{\theta} = -\chi/2, \quad (13)$$

where contributions of the mesoscale ( $e$ ) and microscale ( $t$ ) are separated from the long-term average (denoted by the overbar). Employing down-gradient closures for the diapycnal and isopycnal eddy stirring terms, (4) and (7), then

$$-\kappa_{dia} \left| \frac{\partial \bar{\theta}}{\partial z} \right|^2 - \kappa_{iso} \left| \nabla_\sigma \bar{\theta} \right|^2 = -\chi/2, \quad (14)$$

which allows the isopycnal diffusivity,  $\kappa_{iso}$ , to be diagnosed using

$$\kappa_{iso} = \frac{\chi/2 - \kappa_{dia} \left| \frac{\partial \bar{\theta}}{\partial z} \right|^2}{\left| \nabla_\sigma \bar{\theta} \right|^2}. \quad (15)$$

An example of this diagnostic method applied to a single station is shown in Appendix A.



The isopycnal diffusivity,  $\kappa_{iso}$ , is estimated within different neutral density bins, using  $\chi$  and  $\epsilon$  from 30 VMP-6000 casts,  $N^2$  from the CTD casts adjacent to the VMP deployments, and large-scale potential temperature gradients estimated either across density surfaces from the CTD sections or along density surfaces in the World Ocean Atlas climatology (Locarnini et al., 2013; Zweng et al., 2013). Unphysical values of  $\kappa_{iso}$  are removed from the data, based upon the occurrence of either negative  $\kappa_{iso}$  (where  $\chi$  is less than the production of temperature variance) or near-zero isopycnal temperature gradients (less than a magnitude of  $5 \times 10^{-7} \text{ }^\circ\text{C m}^{-1}$ ).

The resulting estimates of isopycnal diffusivity typically range from 1000 to 4000  $\text{m}^2\text{s}^{-1}$  along the ridge (Figure 3b, blue line). Isopycnal stirring rates are weaker off the ridge, typically by a factor of 2 to 4 (Figure 3b, red line). There is a similar enhancement in diapycnal and isopycnal diffusivity on the ridge for densities greater than 26, which is probably a result of the enhanced tidal mixing there (Vic et al., 2018; Tuerena et al., 2019).

#### 4.4. Isopycnal Diffusivity From a Mixing-Length Approach

The isopycnal diffusivity,  $\kappa_{iso}$ , is also estimated using a mixing-length approach based upon assumed quasi-geostrophic dynamics (Ferrari & Nikurashin, 2010). This estimate entails a two-stage process. First, the isopycnal diffusivity in the absence of a mean flow,  $\kappa_{iso,0}$ , is estimated from the horizontal scale over which mesoscale eddy stirring is predicted to operate,  $k^{-1}$ , related to perturbations in sea surface height,  $h'$ , and to eddy kinetic energy,  $EKE$ ,

$$\kappa_{iso,0} = d_1 \frac{g}{|f|} (h'^2)^{1/2} = \frac{1}{2} d_0 k^{-1} EKE^{1/2}, \quad (16)$$

where  $d_0$  and  $d_1$  are empirically-derived coefficients, linked to the decorrelation time scale, which have been applied in different dynamical regimes of the Southern Ocean (Ferrari & Nikurashin, 2010). Second, the isopycnal diffusivity in the presence of a mean flow,  $\kappa_{iso}$ , is expressed as a modification to the diffusivity without a mean flow (Naveira Garabato et al., 2011),

$$\kappa_{iso} = \frac{\kappa_{iso,0}}{1 + d_2 U_0^2 EKE^{-1}}, \quad (17)$$

where  $d_2$  is an empirically-derived coefficient, linking the phase speed of generated eddies to the mean flow, and  $U_0$  is the background mean flow velocity. An alternative account for the suppression entails the replacement of the mean flow speed ( $U_0$ ) with the Rossby wave speed ( $c_w$ ) (Klocker & Abernathy, 2014).

The isopycnal diffusivity in (17) is evaluated using a combination of altimetric data and mooring observations, by following this procedure:

- (i) The mixing length scale  $k^{-1}$  is estimated from altimetry by comparing the diffusivity derived from sea surface height to the EKE (16) based upon a daily-gridded altimetric product with 1/4 degree horizontal resolution between September 2015 and June 2017;
- (ii) A profile of the isopycnal diffusivity in the absence of a mean flow,  $\kappa_{iso,0}$  (16) is diagnosed from a profile of EKE (derived from mooring-based horizontal velocity data processed with a 40-hour low-pass Butterworth filter) combined with the mixing-length scale in (i) averaged in a 1-degree box around the mooring;
- (iii) A profile of the isopycnal diffusivity in the presence of the mean flow,  $\kappa_{iso}$ , is calculated (17) using the output of (ii), plus the mooring-based estimates of the mean flow and EKE, and coefficients derived by Ferrari and Nikurashin (2010).

At the site of the mooring, EKE reaches just over  $0.007 \text{ m}^2\text{s}^{-2}$  close to the surface, where the mean flow speed is  $2.9 \text{ cm s}^{-1}$ . Both EKE and mean flow speed decrease rapidly over a depth scale of 500 m to  $0.0036 \text{ m}^2\text{s}^{-2}$  and  $0.5 \text{ cm s}^{-1}$ , respectively (Figures 5a and 5b). The first baroclinic Rossby wave speed for this location is given by  $c_w = -\beta L_d^2$ , where  $\beta$  is the meridional gradient in the Coriolis parameter and  $L_d$  is the first baroclinic mode Rossby deformation radius. Taking typical values for these inputs at the mooring site,  $\beta = 1.8 \times 10^{-11} \text{ m}^{-1}\text{s}^{-1}$  and  $L_d = 30 \text{ km}$  (Tulloch et al., 2009), gives a wave speed of  $c_w = 1.6 \text{ cm s}^{-1}$ . This speed is comparable to the mean flow speeds shown by the mooring (Figure 5b), implying that the suppression is not strongly sensitive to the choice between the mean flow and Rossby wave speeds. The isopycnal diffusivity peaks at  $1550 \text{ m}^2\text{s}^{-1}$  at the surface and reduces to typically  $630 \text{ m}^2\text{s}^{-1}$  at a depth of 1000 m (Figure 5c, black line).

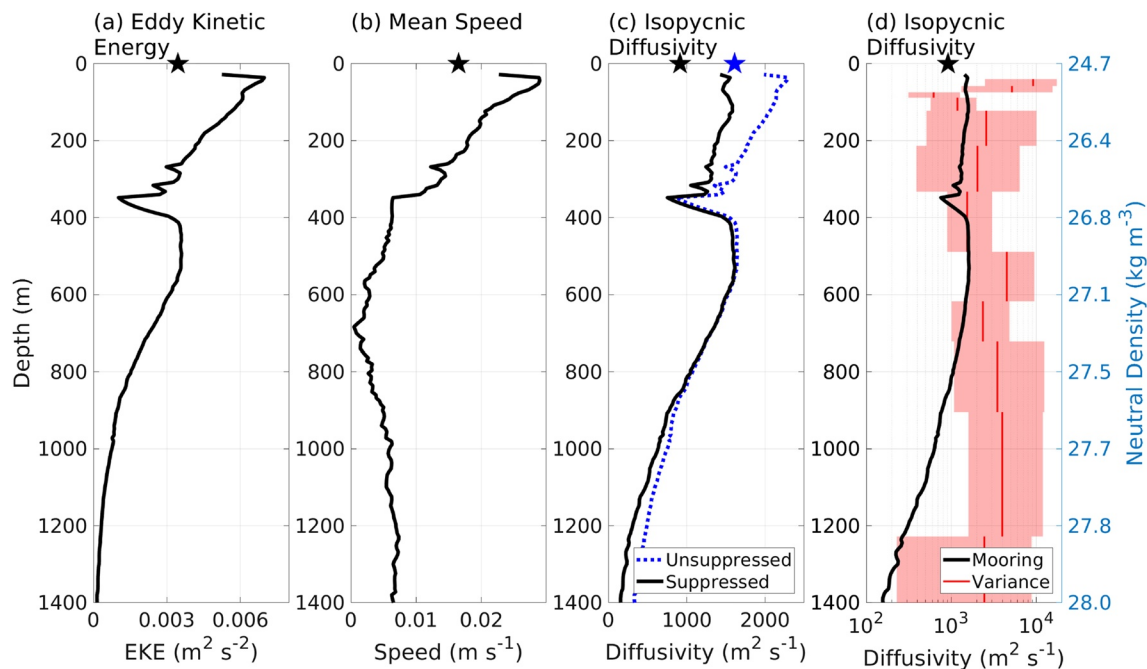


**Figure 5.** Profiles from the mooring (lines) and surface estimates from altimetry (stars) of: (a) eddy kinetic energy, (b) the time-mean velocity, (c) the isopycnal diffusivity in the absence (blue dashed line) and presence (black line) of the mean flow, and (d) the isopycnal diffusivity from the mooring with mean flow (black line) and the isopycnal diffusivity on the ridge calculated using the temperature variance approach (red lines and boxes). The diffusivity from temperature variance is remapped using the median depth of the density surface across the survey.

#### 4.5. Comparison With Other Estimates of Isopycnal Diffusivity From Eddy Stirring

In this study, the effect of mesoscale eddies in providing an isopycnal diffusivity has been estimated for the North Atlantic subtropical gyre using two independent methods, one utilizing a tracer variance approach and the other founded on mixing length theory. Both estimates indicate a maximum isopycnal diffusivity near the surface of approximately 2000 to 4000  $\text{m}^2 \text{s}^{-1}$ , characteristically decaying with depth to 500 to 2000  $\text{m}^2 \text{s}^{-1}$  off and on ridge, respectively. The mixing length estimates are typically slightly lower than the temperature variance estimates, although they are indistinguishable within error envelopes for most depth bins (Figure 5d).

There have been a range of investigations of isopycnal diffusivity in the Northeast Atlantic, particularly in the region of the Mediterranean outflow, that yield diffusivity estimates at 250 m of 800 to 1400  $\text{m}^2 \text{s}^{-1}$  based on measurements of thermohaline variability (Joyce et al., 1998) and of order 1000  $\text{m}^2 \text{s}^{-1}$  from a tracer release experiment (Ledwell et al., 1998). Similar estimates of the diffusivity, 1100  $\text{m}^2 \text{s}^{-1}$  near the surface and 100 to 300  $\text{m}^2 \text{s}^{-1}$  at depth, have been made for the region on the basis of conservation of salt and temperature (Zika & McDougall, 2008; Zika et al., 2010).

There have also been a range of global estimates of the isopycnal diffusivity that are broadly in line with our diagnostics. Theoretical arguments applied to a global climatology at the location of our mooring imply an isopycnal diffusivity that reaches a surface maximum of 1000  $\text{m}^2 \text{s}^{-1}$  and decays to 400  $\text{m}^2 \text{s}^{-1}$  at 1000 m depth (Groeskamp et al., 2020). Global surface calculations give an approximate surface diffusivity of 1000 to 2000  $\text{m}^2 \text{s}^{-1}$  for our region, using separation of surface floats (Roach et al., 2018) and altimetry (Abernathey & Marshall, 2013; Klocker & Abernathey, 2014). Isopycnal diffusivities of 500 to 1500  $\text{m}^2 \text{s}^{-1}$  at 1000 m depth are given by Argo float observations, both from float separation statistics (Roach et al., 2018) and thermohaline distributions in combination with model velocities (Cole et al., 2015).

Thus, the results presented in this study are broadly consistent, in terms of both magnitude and vertical structure, with isopycnal diffusivity estimates from a range of previous studies.

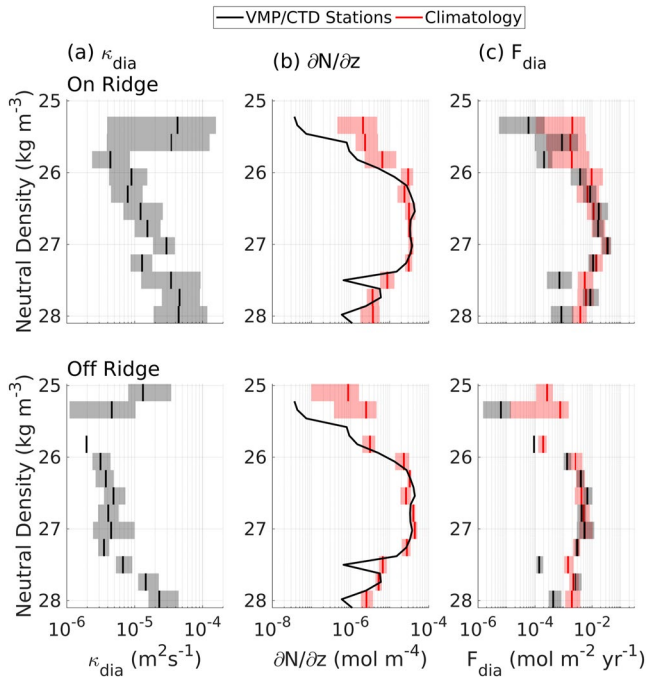


**Figure 6.** The diapycnal component of the vertical diffusive nitrate flux,  $F_{dia}$ , plotted versus neutral density, for the on-ridge (upper row) and off-ridge (lower row) stations: (a) diapycnal diffusivity,  $\kappa_{dia}$  ( $\text{m}^2\text{s}^{-1}$ ), (b) nitrate gradient directed across density surfaces,  $\partial N/\partial z$  ( $\text{mol N m}^{-4}$ ), and (c)  $F_{dia}$  ( $\text{mol N m}^{-2}\text{yr}^{-1}$ ). The black lines show the mean values derived from the microstructure data and the cruise-observed gradients. The red lines are estimates for which the gradients have been derived from climatological data. The shaded regions indicate 95% confidence ranges using a bootstrap method.

$\text{N m}^{-2}\text{yr}^{-1}$  at  $\gamma = 26.5$  to  $27.2$  (Figure 6c). This density variation of  $F_{dia}$  resembles the variation of  $\partial N/\partial z$  more closely than that of  $\kappa_{dia}$ .

Estimates of the diapycnal component of the vertical nitrate flux,  $F_{dia}$ , decrease in magnitude off the ridge by a factor of typically 2 to 3, due to the smaller diapycnal diffusivity,  $\kappa_{dia}$ , there (Tuerena et al., 2019). The estimates of  $F_{dia}$  increase slightly in magnitude if the nitrate gradients are taken from climatology (Figure 6b, red lines) rather than from the cruise observations.

## 5.2. Diapycnal Advective Nitrate Fluxes

On the ridge, the diapycnal advection,  $w^*$ , is relatively large and positive, directed towards lighter surfaces at  $\gamma = 25.6$  and becomes smaller and negative, directed towards denser surfaces at  $\gamma = 27$  (Figure 7a). The accompanying nitrate concentrations are close to zero on the density surfaces lighter than  $\gamma = 26$  and become largest around  $\gamma = 27.4$  (Figure 7b). Consequently, the diapycnal advection of nutrients is small on lighter surfaces and becomes negative at  $\gamma = 27.2$  (Figure 7c). There are, however, large errors in this estimate arising from the estimate of  $w^*$  and the dependence on vertical gradients in  $\kappa_{dia}$ .

Off the ridge, the diapycnal advection,  $w^*$ , is again positive on lighter surfaces at  $\gamma = 26.5$  and negative on denser surfaces at  $\gamma = 27.2$ . The diapycnal advection is an order of magnitude weaker off the ridge, and the upwelling extends onto denser surfaces compared with on the ridge. The vertical structure of the nitrate is similar to that on the ridge. The diapycnal advection of nutrients is then small and positive on lighter surfaces at  $\gamma = 26.6$  and changes to negative at  $\gamma = 27.2$  (Figure 7c). There are again large errors associated with the diapycnal velocity calculation, which is carried through to the nitrate flux.

## 5. Nutrient Supply by Diapycnal Mixing, Diapycnal Advection, and Isopycnal Eddy Stirring

The estimates of the diapycnal and isopycnal diffusivities, respectively, associated with microscale turbulence and mesoscale eddies, and the diapycnal advection, are next combined with the nitrate data to assess their relative roles in nutrient supply to the upper layers of the North Atlantic subtropical gyre. Here, we focus on the contributions of three terms in the nutrient budget: the vertical convergences in the diapycnal diffusion, diapycnal advection, and isopycnal diffusion (see Section 2.2):

$$\underbrace{(\overline{F_{dia}}|_{bot} - \overline{F_{dia}}|_{top})/\overline{h}}_{\text{diapycnal diffusion}}, \quad \underbrace{((\overline{w^*N})|_{bot} - (\overline{w^*N})|_{top})/\overline{h}}_{\text{diapycnal advection}}, \quad (18)$$

and

$$\underbrace{(\mathbf{S}/\overline{h}) \cdot \left( \frac{\partial}{\partial z} (\overline{h\kappa_{iso}} \nabla_{\sigma} \overline{N}) \right)}_{\text{isopycnal diffusion}}.$$

These analyses were also applied to phosphate and lead to broadly similar inferences (not shown here) and the details of the calculation of the gradients are provided in Appendix B.

### 5.1. Diapycnal Diffusive Nitrate Fluxes

For the diapycnal contribution to the diffusive nitrate flux,  $F_{dia}$ , the diapycnal diffusivity,  $\kappa_{dia}$ , is estimated from cruise measurements along the ridge, ranging from an upper bound of 4 to  $5 \times 10^{-5} \text{m}^2\text{s}^{-1}$  at  $\gamma = 25.4$  and  $27.8$ , to a lower bound of  $4 \times 10^{-6} \text{m}^2\text{s}^{-1}$  at  $\gamma = 25.8$  (Figure 6a). The diapycnal nitrate gradient,  $\partial N/\partial z$ , varies in the opposite sense, from relatively low values at  $\gamma = 25.4$  and  $27.8$ , to higher gradients between  $\gamma = 26.2$  and  $27.2$  (Figure 6b, black lines for CTD stations). The diapycnal contribution of the diffusive nitrate flux,  $F_{dia}$ , thus varies from lower values of  $6 \times 10^{-5}$  and  $8 \times 10^{-4} \text{mol N m}^{-2}\text{yr}^{-1}$  at  $\gamma = 25.4$  and  $\gamma = 28$ , to higher values of  $2 \times 10^{-2}$  to  $3 \times 10^{-2} \text{mol N m}^{-2}\text{yr}^{-1}$  at  $\gamma = 26.5$  to  $27.2$  (Figure 6c). This density variation of  $F_{dia}$  resembles the variation of  $\partial N/\partial z$  more closely than that of  $\kappa_{dia}$ .

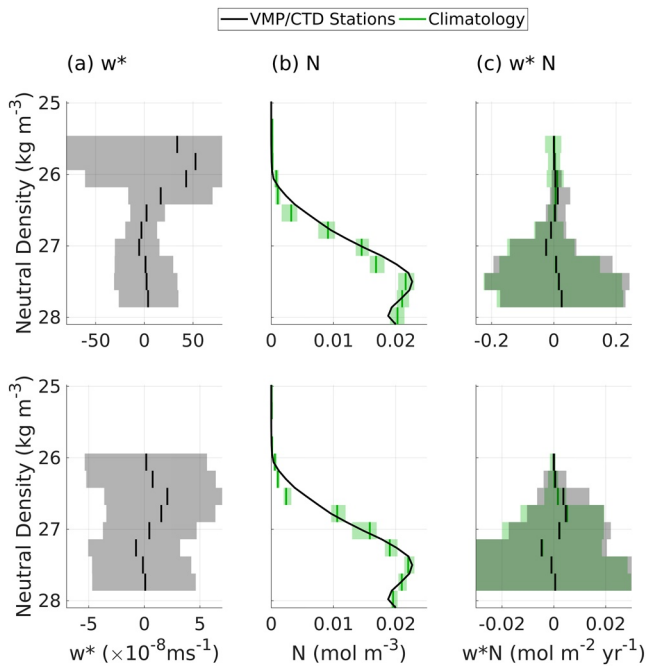


**Figure 7.** The diapycnal advection contribution to the vertical nitrate supply plotted versus neutral density, for the on-ridge (upper row) and off-ridge (lower row) stations. The profiles of (a) diapycnal advection,  $w^*$  ( $\text{m s}^{-1}$ ) directed positive upwards, (b) nitrate concentration on density surfaces,  $N$  ( $\text{mol m}^{-3}$ ), and (c) diapycnal advective nitrate flux,  $w^*N$  ( $\text{mol N m}^{-2}\text{yr}^{-1}$ ). The black lines show the mean values derived from the microstructure data and the cruise-observed gradients. The green lines are estimates for which the gradients have been derived from climatological data. The shaded regions indicate 95% confidence ranges using a bootstrap method.

### 5.3. Isopycnal Diffusive Nitrate Fluxes

For the isopycnal contribution to the diffusive nitrate flux,  $F_{iso}$ , the isopycnal diffusivity,  $\kappa_{iso}$ , is estimated from cruise measurements along the ridge, ranging from an upper bound of  $8 \times 10^3 \text{ m}^2 \text{ s}^{-1}$  at  $\gamma = 25.4$  to a lower bound of  $6 \times 10^2 \text{ m}^2 \text{ s}^{-1}$  at  $\gamma = 25.8$  (Figure 8a). The nitrate gradient along density surfaces,  $\nabla_\sigma N$ , is very low along  $\gamma = 25$  (less than  $10^{-11} \text{ mol N m}^{-4}$ ), and increases to a higher value of typically  $1 \times 10^{-9}$  to  $4 \times 10^{-9} \text{ mol N m}^{-4}$  for  $\gamma = 26.2$  to  $27.8$  (Figure 8b).

The resulting isopycnal contribution to the vertical diffusive nitrate flux,  $F_{iso}$ , ranges from a lower value of  $1.4 \text{ mol N m}^{-2}\text{yr}^{-1}$  along  $\gamma = 25.3$  to an upper value of  $430 \text{ mol N m}^{-2}\text{yr}^{-1}$  along  $\gamma = 27.7$  (Figure 8c). Most of this isopycnal stirring of nitrate is effectively horizontal. However, a small fraction of the stirring is directed vertically and this fraction is given by the isopycnal slope,  $S$ , which typically varies from  $1 \times 10^{-5}$  to  $2 \times 10^{-4}$  (Figure 8d). The resulting isopycnal contribution to the vertical diffusive flux,  $F_{iso}$ , varies between lower values of  $5 \times 10^{-5}$  at  $\gamma = 25.3$  and higher values of  $1.5 \times 10^{-2}$  to  $5.5 \times 10^{-2} \text{ mol N m}^{-2}\text{yr}^{-1}$  at  $\gamma = 26.5$  to  $27.2$  (Figure 8e).

Estimates of  $F_{iso}$  decrease in magnitude off the ridge by a factor of typically 2, due to the smaller isopycnal diffusivity,  $\kappa_{iso}$ , there, linked to the smaller dissipation of thermal variance off the ridge from (15). The estimates of  $F_{iso}$  increase slightly in magnitude if the nitrate gradients are taken from climatology, especially on lighter surfaces.

### 5.4. Vertical Structure of The Nitrate Fluxes and The Seasonal Boundary Layer

The relative importance of the diapycnal and isopycnal contributions to the vertical diffusive nitrate fluxes,  $F_{dia}$  and  $F_{iso}$ , and the diapycnal advection of nitrate,  $w^*N$ , vary with the proximity to the mixed layer and euphotic zone along the ridge, irrespective of whether the nutrients are from climatology or the cruise sections (Figures 9a and 9b).

For light density surfaces that intersect the summer mixed layer and euphotic zone from  $\gamma = 25.2$  to  $26.0$ , the vertical component of the diapycnal diffusive nitrate flux,  $F_{dia}$ , is generally larger than that of the isopycnal diffusive nitrate flux,  $F_{iso}$ . The diapycnal advection is small in the summer surface mixed layer, where the nutrients are generally depleted. For surfaces that intersect the winter mixed layer between  $\gamma = 26.2$  and  $26.8$ , the nutrient transfer components are comparable to each other, sometimes with the diapycnal diffusive component,  $F_{dia}$ , or the isopycnal diffusive component,  $F_{iso}$ , dominating. The diapycnal advective flux,  $w^*N$ , is directed towards lighter surfaces, with this upward transfer being due to the enhanced mixing in the surface boundary layer.

For denser surfaces below the winter mixed layer from  $\gamma = 26.8$ , the isopycnal diffusive nitrate flux,  $F_{iso}$ , is generally larger than the diapycnal diffusive nitrate flux,  $F_{dia}$ , with a maximum value of  $0.055 \text{ mol N m}^{-2}\text{yr}^{-1}$  at  $\gamma = 27$ . The diapycnal advection of nitrate,  $w^*N$ , on denser surfaces close to  $\gamma = 27$ , is negative, and so opposes the diapycnal diffusive and eddy stirring transfers. The diapycnal advection of nitrate is weakly positive on denser surfaces,  $\gamma = 27.5$ , towards the bottom boundary. Hence, the vertical nitrate flux is controlled, by reinforcing contributions from diapycnal diffusion, diapycnal advection, and isopycnal eddy stirring at the base of the summer mixed layer, and by a loss from diapycnal advection and a supply from isopycnal eddy stirring below the seasonal boundary layer.

In comparison, off the ridge, there are smaller diapycnal diffusive nitrate fluxes,  $F_{dia}$ , and smaller diapycnal advective fluxes,  $w^*N$ , due to the weaker tidal mixing (Tuerena et al., 2019). There is a more varied structure, with the vertical component of the isopycnal nitrate flux,  $F_{iso}$ , usually being comparable to or larger than both the diapycnal diffusive nitrate flux and the diapycnal advective flux, with a maximum value of  $0.02 \text{ mol N m}^{-2}\text{yr}^{-1}$  at  $\gamma = 27.5$  (Figures 9c and 9d).

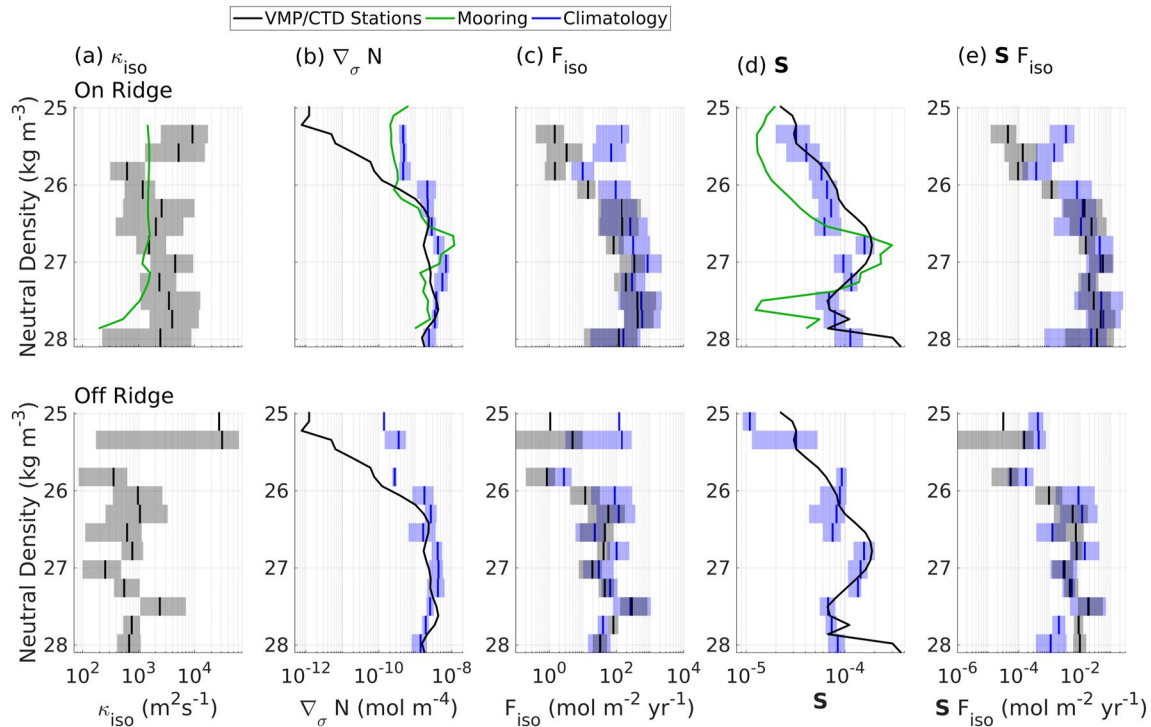


**Figure 8.** The isopycnal stirring contribution to the vertical diffusive nitrate flux plotted versus neutral density, for the on-ridge (upper row) and off-ridge (lower row) stations. The profiles: (a) isopycnal diffusivity,  $\kappa_{iso}$  ( $m^2 s^{-1}$ ), (b) nitrate gradient along density surfaces,  $\nabla_{\sigma} N$  ( $mol N m^{-4}$ ), (c) isopycnal nitrate flux,  $-\kappa_{iso} \nabla_{\sigma} N$  ( $mol N m^{-2} yr^{-1}$ ), (d) slope parallel to density surfaces,  $S$ , and (e) vertical component of the isopycnal nitrate flux,  $S F_{iso}$  ( $mol N m^{-2} yr^{-1}$ ). The black lines show the mean values derived from the microstructure data and the cruise-observed gradients. The blue lines are estimates for which the gradients have been derived from climatological data. The green lines show the mixing length-estimated isopycnal diffusivity based on climatological gradients. The shaded regions indicate 95% confidence ranges using a bootstrap method.

In terms of the seasonality, in winter and into early spring, the nitrate supply to a density layer is likely to be dominated by the isopycnal nitrate transfer as winter mixed layers intersect denser surfaces and there are stronger nutrient gradients. In summer, the diapycnal nitrate transfer instead may dominate as there are weaker isopycnal nitrate gradients. The diapycnal advective flux is likely to increase in autumn and winter as the strong turbulence extends deeper into the water column and the depletion of surface nutrients is reduced.

### 5.5. Vertical Convergence of Nitrate Fluxes

Whether there is a nitrate supply to a density class is determined by the vertical convergence of the vertical nitrate flux. On the ridge, there is generally a positive nitrate supply from the sum of the diapycnal diffusion, diapycnal advection, and isopycnal diffusion of nitrate (Figures 10a and 10b, black crosses).

Within the seasonal boundary layer extending over the summer and winter mixed layers between  $\gamma = 25.6$  and  $26.4$ , there is generally a reinforcing supply of nitrate from the vertical convergence of diapycnal diffusive, diapycnal advective, and isopycnal diffusive components of the vertical nitrate flux (Figures 10a and 10b, red, green, and blue dots).

Below the winter mixed layer within the thermocline, there is instead a loss of nitrate from diapycnal advection,  $w^*N$ , between  $\gamma = 26.8$  and  $27.2$  (Figures 10a and 10b, green dots) and a loss of nitrate from diapycnal mixing,  $F_{dia}$ , at  $\gamma = 27.2$  (Figures 10a and 10b, red dots). These losses of nitrate are though offset by a supply of nitrate from the isopycnal diffusive component,  $F_{iso}$  at  $\gamma = 26.8$  to  $27.2$  (Figures 10a and 10b, blue dots) and by diapycnal advection,  $w^*N$ , on denser surfaces.

Off the ridge, the overall nitrate supply is positive over most  $\gamma$  surfaces, but is negative for  $\gamma = 27.2$  for the climatology, and for  $\gamma = 26.9$  for the cruise section (Figures 10c and 10d, black crosses). Within the seasonal boundary layer for  $\gamma = 25.4$  to  $26.5$ , there is again a supply of nitrate from reinforcing contributions from the diapycnal

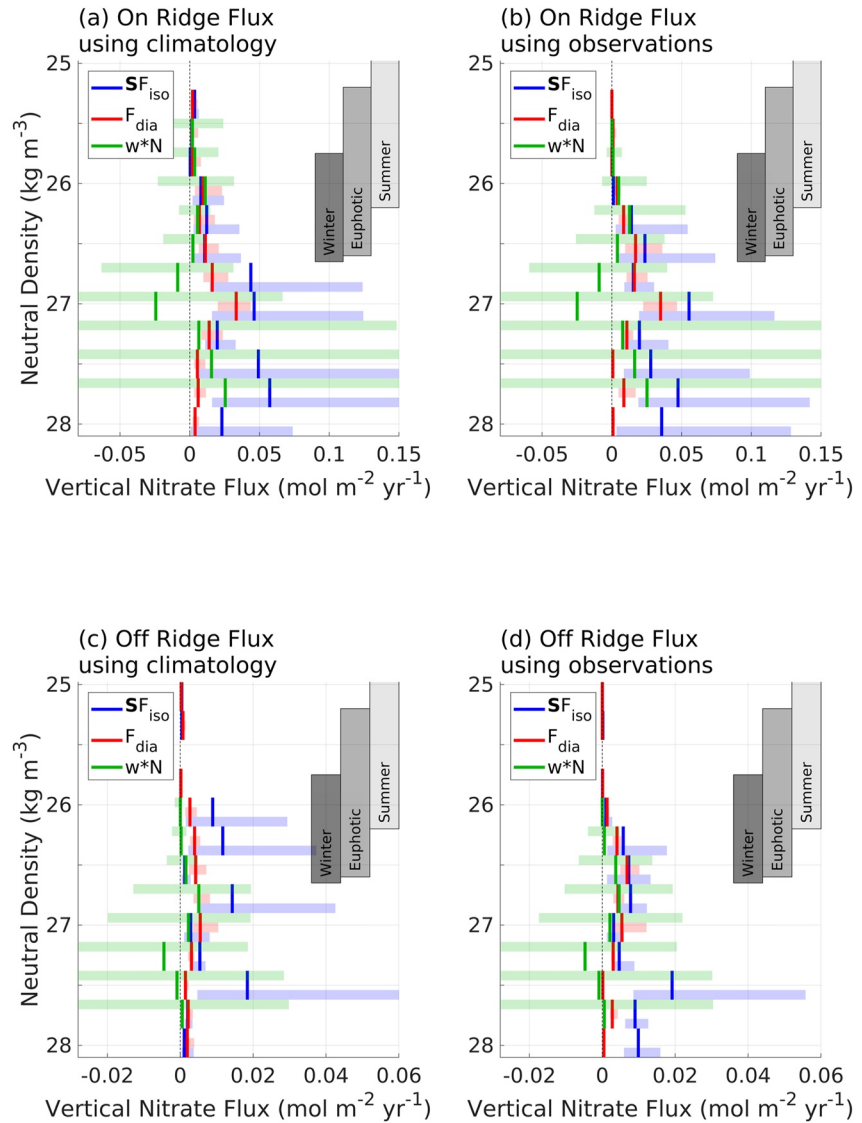


**Figure 9.** Profiles, in neutral density, of the diapycnal diffusion, diapycnal advection, and isopycnal diffusion contributions to the vertical nitrate flux for the on-ridge stations (a and b) and off-ridge stations (c and d), taken from microstructure-derived diffusivities and (a and c) the climatology-derived nutrient gradients or (b and d) the cruise-derived nutrient gradients. Blue shades indicate the isopycnal diffusion contributions, green shades indicate the diapycnal advection contributions, and red shades the diapycnal diffusion contributions. The shaded areas are the 95% confidence intervals derived from a bootstrap method. The grey bars indicate the range of neutral density surfaces in the cruise region representing, from left to right: the base of the summer mixed layer, the base of the summer euphotic zone, and the base of the winter mixed layer.

diffusive and isopycnal components of the vertical nitrate flux,  $F_{dia}$  and  $F_{iso}$ , and the convergence in the diapycnal advection,  $w*N$  (Figures 10c and 10d, red, blue, and green dots). Below the winter mixed layer, for  $\gamma = 27.2$  in the climatology and from  $\gamma = 26.9$  to  $27.3$  in the cruise section, there is instead a loss of nitrate from the convergences of the diapycnal nitrate flux,  $F_{dia}$  and the diapycnal advection of nitrate,  $w*N$ , which is partly offset by a nitrate supply by the convergence of the isopycnal nitrate flux,  $F_{iso}$ .

Hence, the vertical nitrate supply changes from (i) a nitrate supply from reinforcing diapycnal and isopycnal transfers within the seasonal boundary layer, to (ii) a loss of nitrate below the seasonal boundary layer from either the diapycnal diffusion or diapycnal advection of nitrate, which is partly offset by an isopycnal diffusive supply involving the stirring by mesoscale eddies.

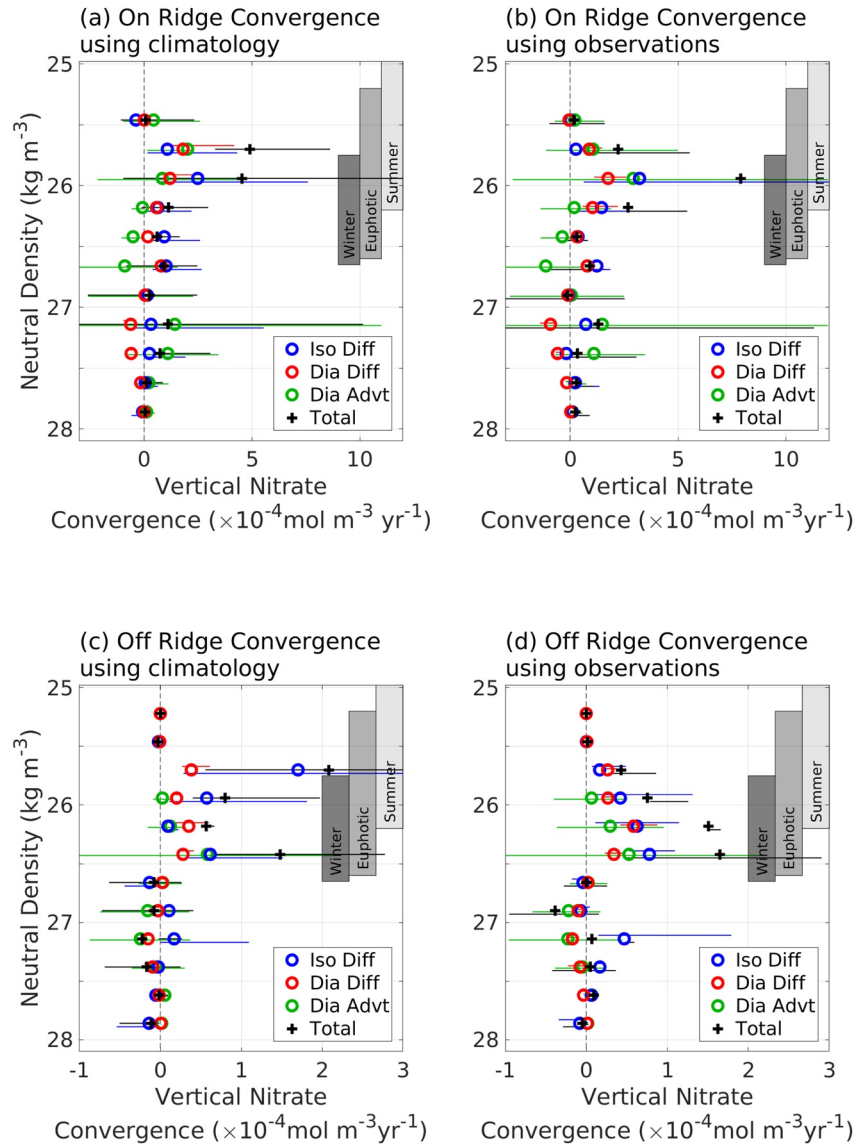


**Figure 10.** Profiles, in neutral density, of the diapycnal diffusion, diapycnal advection, and isopycnal diffusion contributions to the vertical nitrate convergence for the on-ridge stations (a and b) and off-ridge stations (c and d), taken from the microstructure-derived diffusivities and (a and c) the climatology-derived nutrient gradients or (b and d) the cruise-derived nutrient gradients. Blue shades indicate the isopycnal diffusion contributions, green shades indicate the diapycnal advection contributions, and the red shades the diapycnal diffusion contributions. The horizontal lines indicate the 95% confidence intervals derived from a bootstrap method. The grey bars show the range of neutral density surfaces in the cruise region representing, from left to right: the base of the summer mixed layer, the base of the summer euphotic zone, and the base of the winter mixed layer. Convergences of vertical nitrate fluxes are calculated using the median separation of the neutral surfaces over the relevant subset of data, with fluxes that have been smoothed using a 3-span moving average.

## 6. Discussion and Conclusions

There is a problem of understanding how export production is sustained in oligotrophic waters within the extensive downwelling zones of the subtropical gyres. In the Sargasso Sea, tracer-based estimates of export production (Jenkins & Goldman, 1985; Jenkins, 1988; Jenkins & Wallace, 1992; Stanley et al., 2015) exceed by a factor of two or more the combined estimates from nitrate supply from entrainment, Ekman transports, atmospheric deposition, and diapycnal mixing (McGillicuddy et al., 1998; Williams & Follows, 2003). This conundrum might be solved by an enhanced physical supply of nutrients through the effects of transient eddy and frontal

upwelling of nutrients into the euphotic zone (McGillicuddy Jr & Robinson, 1997; McGillicuddy et al., 1998; Lévy et al., 2001, 2012) and regionally-enhanced diapycnal mixing over rough topography (Tuerena et al., 2019). Both these possible physical solutions lead to a new issue, as the time-varying upwelling and diapycnal supply will cease to be effective when the nutrient concentrations in the upper thermocline become eroded (Oschlies, 2002; Williams & Follows, 2003). The resolution of this conundrum might involve the lateral supply of nutrients to the upper thermocline, thereby sustaining nutrient concentrations below the euphotic zone.

The lateral supply of nutrients may be achieved through the time-mean geostrophic flow, although this transfer becomes weak at the gyre boundaries as geostrophic streamlines align with nutrient contours along density surfaces. The Ekman-induced horizontal transport of nutrients does provide an effective supply across time-mean geostrophic streamlines along the flanks of the subtropical gyres (Williams & Follows, 1998), but this supply becomes weak in the upper thermocline and towards the central parts of the gyre. There may also be a transfer of nutrients across the time-mean geostrophic streamlines via a combination of eddy-induced advection and diffusion along density surfaces, as illustrated in idealized eddy-resolving model studies (Lee & Williams, 2000; Lévy, 2008).

In this field-based investigation, which targeted some of the most oligotrophic waters of the North Atlantic subtropical gyre, the relative importance of diapycnal mixing, diapycnal advection, and eddy stirring in supplying nutrients is assessed over the seasonal boundary layer and the thermocline. This region is far from the complicating effects of boundary current flows or areas of strong air-sea interaction, but does lie over the mid-Atlantic ridge, where there is enhanced diapycnal mixing from the spring-neap cycle of the tides interacting with the topography (Vic et al., 2018; Tuerena et al., 2019). In our data analysis, we find that the combination of diapycnal diffusion and diapycnal advection leads to a supply of nutrients to the euphotic zone, but at the same time to a loss of nutrients in the upper thermocline. Isopycnal diffusion from the stirring by mesoscale eddies augment the diapycnal supply of nitrate to the lighter density surfaces intersecting the euphotic zone. This eddy stirring crucially provides nutrients to the upper thermocline and so acts to offset the loss of nutrients associated with the diapycnal transfer. Thus, the eddy-induced lateral transfer of nutrients along density surface may be part of the solution to the long-standing question of how the supply of nutrients to the euphotic zone is sustained.

While our study reveals clear signals of how the eddy stirring acts to augment and partly sustain the diapycnal supply of nutrients, our combined estimates of diapycnal mixing and eddy stirring-driven supply of nitrate at 300 m only reaches 0.03 and 0.05 mol N m<sup>-2</sup> yr<sup>-1</sup> on the ridge for climatological and observed nutrients. Our estimates are thus smaller by a factor of 3 to 4 than estimates of nitrate export of 0.17 mol N m<sup>-2</sup> yr<sup>-1</sup> from oxygen utilization rates (Jenkins, 1987) at a nearby 1000 km triangular site centered at 26.5°N, 32°W. Hence, there is a possibility that the eddy stirring is only providing a modest, background contribution to the nutrient supply to the euphotic zone and upper thermocline.

However, our estimates of the nutrient supply role of eddy stirring are based on a field program at the center of a subtropical gyre and the eddy stirring is expected to provide a larger contribution toward the flanks of the gyre. The eddy stirring supply of nitrate, evaluated from the vertical component of the convergence of the diffusive isopycnal nitrate flux,  $(\mathbf{S}/h) \cdot \partial/\partial z(\bar{h}\kappa_{iso}\nabla_{\sigma}\bar{N})$  in (18), is proportional to the product of the isopycnal diffusivity,  $\kappa_{iso}$ , the isopycnal nitrate gradient,  $\nabla_{\sigma}N$  and the slope of the density surfaces,  $\mathbf{S}$ . Both the nitrate gradient and isopycnal slope are relatively low over our field site in the center of the subtropical gyre (Figures 11a and 11b), as revealed by the climatological distributions of nitrate and density during summer for the  $\gamma = 26.5$  surface, which spans depths of 50 m to 300 m (Garcia et al., 2013). Both of these contributions to the vertical nitrate flux are amplified by a factor of at least 10 on the boundaries of the subtropical gyre (Figures 11c and 11d). The lateral diffusivity associated with eddy stirring is though inhibited toward the surface by the presence of strong flows (Ferrari & Nikurashin, 2010; Groeskamp et al., 2020), which leads to a reduction in  $\kappa_{iso}$  from 500 to 1000 m<sup>2</sup>s<sup>-1</sup> (Groeskamp et al., 2020) in the gyre interior, to 200 m<sup>2</sup>s<sup>-1</sup> over the Gulf Stream (Bower et al., 1985; Abernathy & Marshall, 2013).

While our field study has by necessity focused on the vertical component of the mesoscale eddy-induced diffusive transfer of nutrients, eddies also provide a lateral advective transfer of nutrients, which may be important in transferring nutrients across gyre boundaries (Lee & Williams, 2000; Williams & Follows, 2003) and augment the lateral nutrient supply by the horizontal Ekman transport (Williams & Follows, 1998; Letscher et al., 2016).

In summary, the nutrient supply to the euphotic zone in the center of the oligotrophic subtropical gyre may be achieved via a multistage mechanism: a diapycnal transfer of nutrients by microscale turbulence to the euphotic



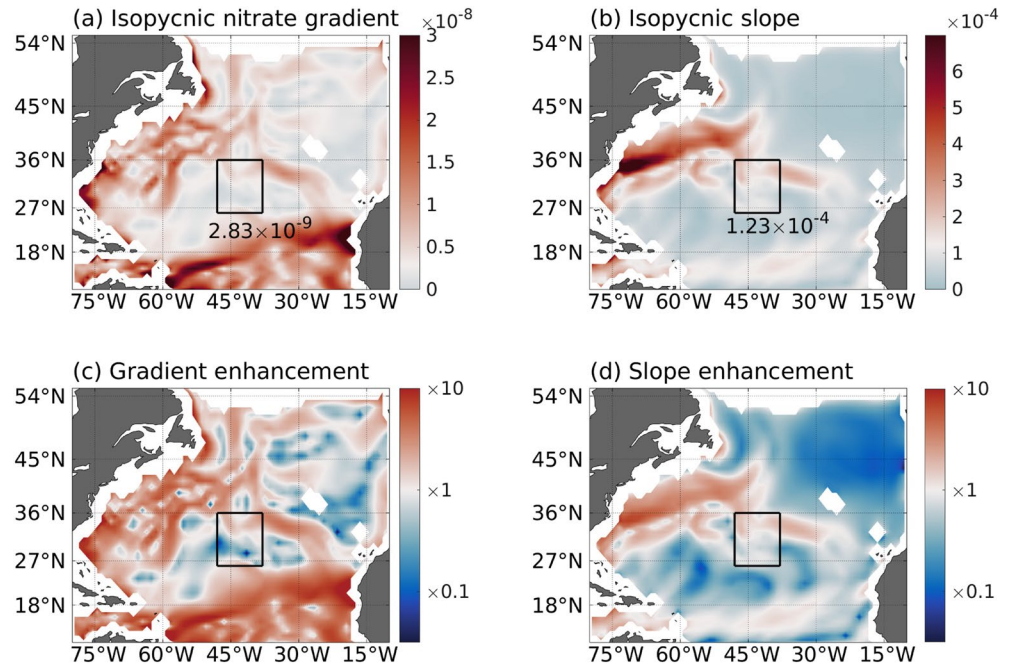


**Figure 11.** Maps showing (a) the magnitude of the isopycnal gradients of nitrate,  $|\nabla_{\sigma} N|$  (mol  $m^{-4}$ ), (b) the slope of the isopycnal surfaces,  $S$ , and in (c) and (d), the enhancement relative to the study region for (a) and (b). The nitrate and density fields are taken from the summer World Ocean Atlas climatology along the  $\gamma = 26.5$  surface. The black box represents the region of our observations and the numbers are the average within that box.

zone from the upper thermocline, and an isopycnal transfer of nutrients by mesoscale eddies acting to both augment the supply to the euphotic zone and replenish upper thermocline nutrients. The wider generality of our central result is suggested by the similar multistage process uncovered in a modelling study of the Southern Ocean supply of trace metals (Uchida et al., 2020), whereby eddy stirring was found to replenish the thermocline and diapycnal mixing to provide the transfer to the euphotic zone.

### Appendix A: Estimates of Diffusivity From Station Data

Following Naveira Garabato et al. (2016), the production and the dissipation of the temperature variance is estimated from the CTD/VMP stations, allowing the isopycnal diffusivity to be diagnosed as a residual,

$$\kappa_{iso} = \frac{\langle \chi \rangle / 2 - \Gamma \epsilon N^{-2} \left| \frac{\partial \theta_m}{\partial z} \right|^2}{|\nabla_{\sigma} \theta_m|^2}. \quad (A1)$$

The dissipation of the temperature variance for a single station usually exceeds the production term from the microscale turbulence (Figure A1c), taken from the combination of the diapycnal diffusivity and temperature gradients (Figures A1a and A1b). With the addition of the isopycnal temperature gradients (Figure A1d), the diffusivity for a single station can then be calculated (Figure A1e).

### Appendix B: Calculation of Isopycnal Slopes and Gradients

Isopycnal gradients of potential temperature and nutrient are taken both from observations and from a climatology. The methodology is set out due to complexities of evaluating these gradients on isopycnal or neutral surfaces (Groeskamp, Barker, et al., 2019).

For the observations, each cast is linearly interpolated in the vertical onto a consistent neutral density grid (Jackett & McDougall, 1997) with a spacing of  $0.12 \text{ kg m}^{-3}$ , such that each cast has a profile of depth, potential temperature, and nitrate in neutral density space. This interpolation avoids making a local assumption in calculating gradients from the combination of horizontal and vertical gradients. All subsequent calculations are then performed

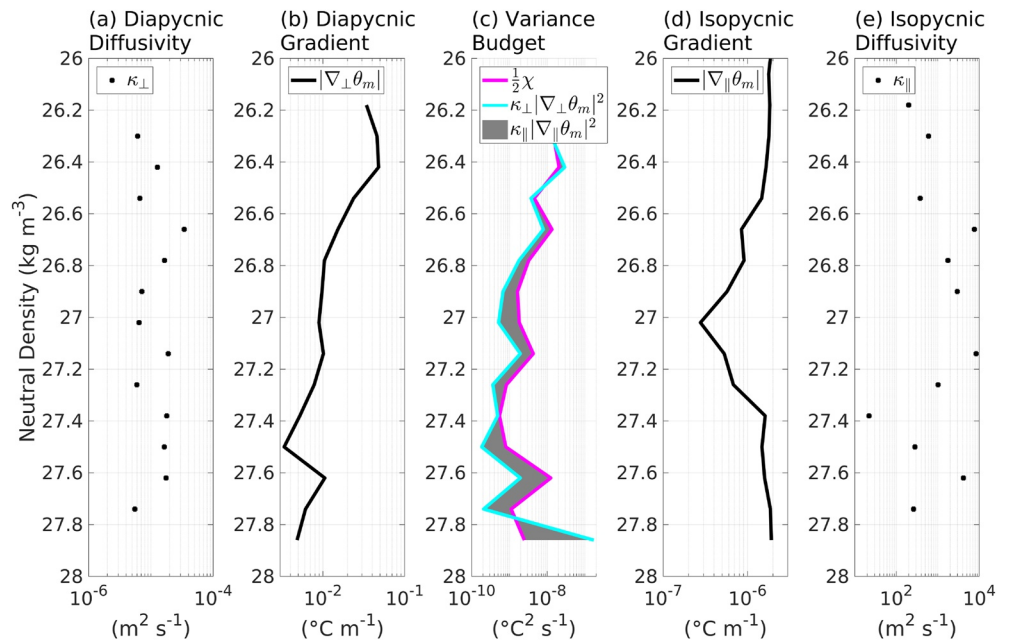


**Figure A1.** Profiles at a single station in neutral density space of: (a) the diapycnic diffusivity; (d) absolute temperature gradients across density surfaces; (c) temperature variance dissipation (cyan line) and temperature variance production by diapycnic mixing (magenta line) with the shaded area indicating the production by isopycnic stirring; (d) absolute temperature gradients along density surfaces; and (e) the diffusivity along density surfaces.

on the same neutral density grid. For each value of neutral density, a flat surface (linear in  $x$  and  $y$  directions) is fitted using distance north and east from a fixed position for each variable (Figure B1). The zonal and meridional gradients in depth, potential temperature and nitrate, are then extracted from these fitted surfaces. These surfaces effectively smooth over the local gradients driven by mesoscale processes and provides gradients representative of the size of the survey of the order of 1000 km.

For the climatology, individual profiles are again remapped onto a consistent neutral density grid using the routines of (Jackett & McDougall, 1997). It is assumed that in the construction of the climatology, the gradients associated with mesoscale features are already removed, so that local gradients are used. The gradients are taken

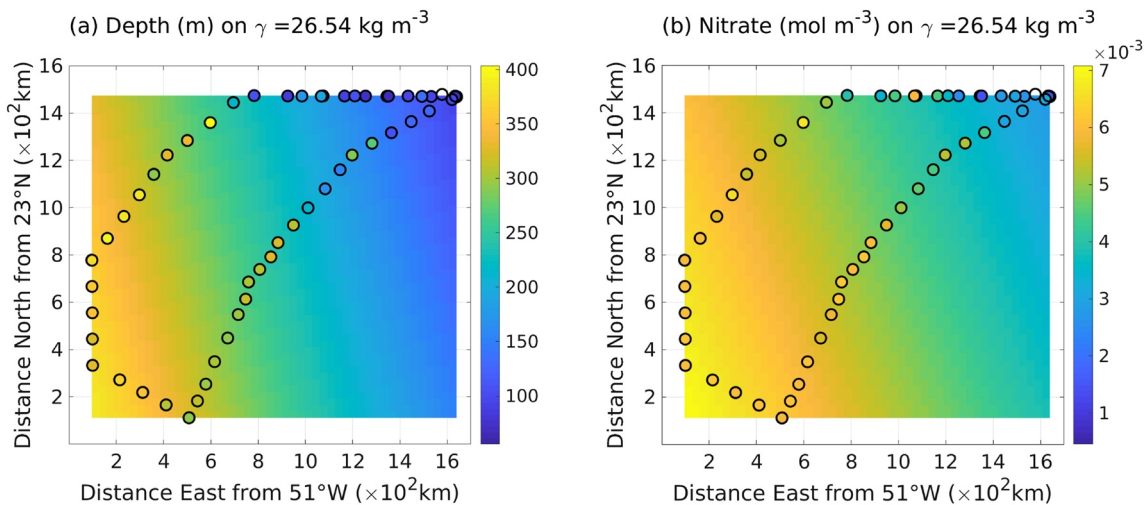


**Figure B1.** Maps showing the fitted surfaces of depth (slope) and nitrate for the surface  $\gamma = 26.54 \text{ kg m}^{-3}$ . The observations, interpolated onto the density surface, are shown by the circles. The background color shows the fitted surface from which the gradients are extracted.

on the same grid as the climatology using centered differencing, such that the resulting gradients are taken over twice the horizontal spacing of the climatology resolution. These gradients are then applied to the observations using the closest position in the climatology grid.

## Data Availability Statement

The hydrographic, turbulence, and inorganic nutrient data are freely available via the British Oceanographic Data Centre: Vic et al. (2018) has published the hydrographic and turbulence data, and the nutrient data are available in Tuerena and Mahaffey (2021), doi: [10.5285/b9bd0df2-f8de-21fe-e053-6c86abc0cb35](https://doi.org/10.5285/b9bd0df2-f8de-21fe-e053-6c86abc0cb35).

## Acknowledgments

RidgeMix was supported by the U.K. Natural Environment Research Council (NE/L004216/1). We are grateful to the technicians, officers, and crew of RRS James Clark Ross for their invaluable role in data collection. We thank Claire Mahaffey and Clare Davis for support with biogeochemical measurements and Malcolm Woodward for use of the nutrient analyzer at sea. We are grateful to Trevor McDougall for pointing out the importance of the diapycnal advection term, which had been omitted in a previous version of this work, and to Ryan Abernathy and an anonymous referee for positive comments that have strengthened the study.

## References

- Abernathy, R. P., & Marshall, J. (2013). Global surface eddy diffusivities derived from satellite altimetry. *Journal of Geophysical Research: Oceans*, *118*, 901–916. <https://doi.org/10.1002/jgrc.20066>
- Bleck, R. (1998). Ocean modeling in isopycnic coordinates. In *Ocean modeling and parameterization* (pp. 423–448). Springer. [https://doi.org/10.1007/978-94-011-5096-5\\_18](https://doi.org/10.1007/978-94-011-5096-5_18)
- Bleck, R., & Boudra, D. B. (1981). Initial testing of a numerical ocean circulation model using a hybrid(quasi-isopycnic) vertical coordinate. *Journal of Physical Oceanography*, *11*(6), 755–770. [https://doi.org/10.1175/1520-0485\(1981\)011<0755:itoano>2.0.co;2](https://doi.org/10.1175/1520-0485(1981)011<0755:itoano>2.0.co;2)
- Bower, A. S., Rossby, H. T., & Lillibridge, J. L. (1985). The Gulf Stream—barrier or blender? *Journal of Physical Oceanography*, *15*, 24–32. [https://doi.org/10.1175/1520-0485\(1985\)015<0024:tgsob>2.0.co;2](https://doi.org/10.1175/1520-0485(1985)015<0024:tgsob>2.0.co;2)
- Canuto, V., & Dubovikov, M. (2011). Comparison of four mixed layer mesoscale parameterizations and the equation for an arbitrary tracer. *Ocean Modelling*, *39*(1–2), 200–207. <https://doi.org/10.1016/j.ocemod.2011.04.008>
- Cole, S. T., Wortham, C., Kunze, E., & Owens, W. B. (2015). Eddy stirring and horizontal diffusivity from Argo float observations: Geographic and depth variability. *Geophysical Research Letters*, *42*, 3989–3997. <https://doi.org/10.1002/2015gl063827>
- de Lavergne, C., Madec, G., Le Sommer, J., Nurser, A. G., & Garabato, A. C. N. (2016). On the consumption of Antarctic bottom water in the abyssal ocean. *Journal of Physical Oceanography*, *46*, 635–661. <https://doi.org/10.1175/jpo-d-14-0201.1>
- Dietze, H., Oschlies, A., & Kähler, P. (2004). Internal-wave-induced and double-diffusive nutrient fluxes to the nutrient-consuming surface layer in the oligotrophic subtropical North Atlantic. *Ocean Dynamics*, *54*(1), 1–7. <https://doi.org/10.1007/s10236-003-0060-9>
- Ferrari, R., & Nikurashin, M. (2010). Suppression of eddy diffusivity across jets in the Southern Ocean. *Journal of Physical Oceanography*, *40*, 1501–1519. <https://doi.org/10.1175/2010jpo4278.1>
- Ferrari, R., & Polzin, K. L. (2005). Finescale structure of the T–S relation in the eastern North Atlantic. *Journal of Physical Oceanography*, *35*(8), 1437–1454. <https://doi.org/10.1175/jpo2763.1>
- Garcia, H. E., Locarnini, R. A., Boyer, T. P., Antonov, J. I., Baranova, O. K., Zweng, M. M., & Johnson, D. R. (2013). In S. Levitus, & A. V. Mishonov (Eds.), *World Ocean Atlas 2013 volume 4: Dissolved inorganic nutrients (phosphate, nitrate, silicate)*.
- Gent, P. R., & McWilliams, J. C. (1990). Isopycnal mixing in ocean circulation models. *Journal of Physical Oceanography*, *20*(1), 150–155. [https://doi.org/10.1175/1520-0485\(1990\)020<0150:imiocm>2.0.co;2](https://doi.org/10.1175/1520-0485(1990)020<0150:imiocm>2.0.co;2)
- Gent, P. R., Willebrand, J., McDougall, T. J., & McWilliams, J. C. (1995). Parameterizing eddy-induced tracer transports in ocean circulation models. *Journal of Physical Oceanography*, *25*(4), 463–474. [https://doi.org/10.1175/1520-0485\(1995\)025<0463:peitti>2.0.co;2](https://doi.org/10.1175/1520-0485(1995)025<0463:peitti>2.0.co;2)
- Gregg, M., D’Asaro, E., Riley, J., & Kunze, E. (2018). Mixing efficiency in the ocean. *Annual Review of Marine Science*, *10*, 443–473. <https://doi.org/10.1146/annurev-marine-121916-063643>
- Groeskamp, S., Barker, P. M., McDougall, T. J., Abernathy, R. P., & Griffies, S. M. (2019). Venm: An algorithm to accurately calculate neutral slopes and gradients. *Journal of Advances in Modeling Earth Systems*, *11*, 1917–1939. <https://doi.org/10.1029/2019ms001613>
- Groeskamp, S., Griffies, S. M., Iudicone, D., Marsh, R., Nurser, A. G., & Zika, J. D. (2019). The water mass transformation framework for ocean physics and biogeochemistry. *Annual review of marine science*, *11*, 271–305. <https://doi.org/10.1146/annurev-marine-010318-095421>
- Groeskamp, S., LaCasce, J. H., McDougall, T. J., & Rogé, M. (2020). Full-depth global estimates of ocean mesoscale eddy mixing from observations and theory. *Geophysical Research Letters*, *47*(18), e2020GL089425. <https://doi.org/10.1029/2020gl089425>
- Jackett, D. R., & McDougall, T. J. (1997). A neutral density variable for the World’s Oceans. *Journal of Physical Oceanography*, *27*, 237–263. [https://doi.org/10.1175/1520-0485\(1997\)027<0237:andvft>2.0.co;2](https://doi.org/10.1175/1520-0485(1997)027<0237:andvft>2.0.co;2)
- Jenkins, W. (1987). <sup>3</sup>H and <sup>3</sup>He in the Beta Triangle: Observations of gyre ventilation and oxygen utilization rates. *Journal of Physical Oceanography*, *17*(6), 763–783. [https://doi.org/10.1175/1520-0485\(1987\)017<0763:aitbo>2.0.co;2](https://doi.org/10.1175/1520-0485(1987)017<0763:aitbo>2.0.co;2)
- Jenkins, W. (1988). Nitrate flux into the euphotic zone near Bermuda. *Nature*, *331*(6156), 521–523. <https://doi.org/10.1038/331521a0>
- Jenkins, W., & Goldman, J. (1985). Seasonal oxygen cycling and primary production in the Sargasso Sea. *Journal of Marine Research*, *43*(2), 465–491. <https://doi.org/10.1357/002224085788438702>
- Jenkins, W., & Wallace, D. (1992). Tracer based inferences of new primary production in the sea. In *Primary productivity and biogeochemical cycles in the sea* (pp. 299–316). Springer. [https://doi.org/10.1007/978-1-4899-0762-2\\_17](https://doi.org/10.1007/978-1-4899-0762-2_17)
- Joyce, T. M., Luyten, J. R., Kubryakov, A., Bahr, F. B., & Pallant, J. S. (1998). Meso- to large-scale structure of subducting water in the subtropical gyre of the eastern North Atlantic Ocean. *Journal of Physical Oceanography*, *28*, 40–61. [https://doi.org/10.1175/1520-0485\(1998\)028<0040:mtlssso>2.0.co;2](https://doi.org/10.1175/1520-0485(1998)028<0040:mtlssso>2.0.co;2)
- Klocker, A., & Abernathy, R. (2014). Global patterns of mesoscale eddy properties and diffusivities. *Journal of Physical Oceanography*, *44*(3), 1030–1046. <https://doi.org/10.1175/jpo-d-13-0159.1>
- Klocker, A., & McDougall, T. J. (2010). Influence of the nonlinear equation of state on global estimates of diapycnal advection and diffusion. *Journal of Physical Oceanography*, *40*(8), 1690–1709. <https://doi.org/10.1175/2010jpo4303.1>
- Knap, A., Jickells, T., Pszeny, A., & Galloway, J. (1986). Significance of atmospheric-derived fixed nitrogen on productivity of the Sargasso Sea. *Nature*, *320*(6058), 158–160. <https://doi.org/10.1038/320158a0>
- Kunze, E., Firing, E., Hummon, J. M., Chereskin, T. K., & Thurnherr, A. M. (2006). Global abyssal mixing inferred from lowered ADCP shear and CTD strain profiles. *Journal of Physical Oceanography*, *7*, 1553–1576. <https://doi.org/10.1175/jpo2926.1>
- Ledwell, J. R., Watson, A. J., & Law, C. S. (1998). Mixing of a tracer in the pycnocline. *Journal of Geophysical Research*, *103*, 21499–21529. <https://doi.org/10.1029/98jc01738>

- Lee, M.-M., Marshall, D. P., & Williams, R. G. (1997). On the eddy transfer of tracers: Advective or diffusive? *Journal of Marine Research*, 55(3), 483–505. <https://doi.org/10.1357/0022240973224346>
- Lee, M.-M., & Williams, R. G. (2000). The role of eddies in the isopycnal transfer of nutrients and their impact on biological production. *Journal of Marine Research*, 58(6), 895–917. <https://doi.org/10.1357/002224000763485746>
- Letscher, R. T., Primeau, F., & Moore, J. K. (2016). Nutrient budgets in the subtropical ocean gyres dominated by lateral transport. *Nature Geoscience*, 9(11), 815–819. <https://doi.org/10.1038/ngeo2812>
- Lévy, M. (2008). The modulation of biological production by oceanic mesoscale turbulence. *Transport and mixing in geophysical flows*, 219–261.
- Lévy, M., Ferrari, R., Franks, P. J., Martin, A. P., & Rivière, P. (2012). Bringing physics to life at the submesoscale. *Geophysical Research Letters*, 39(14). <https://doi.org/10.1029/2012gl052756>
- Lévy, M., Klein, P., & Treguier, A.-M. (2001). Impact of sub-mesoscale physics on production and subduction of phytoplankton in an oligotrophic regime. *Journal of marine research*, 59(4), 535–565. <https://doi.org/10.1357/002224001762842181>
- Lewis, M. R., Hebert, D., Harrison, W. G., Platt, T., & Oakey, N. S. (1986). Vertical nitrate fluxes in the oligotrophic ocean. *Science*, 234(4778), 870–873. <https://doi.org/10.1126/science.234.4778.870>
- Locarnini, R. A., Mishonov, A. V., Antonov, J. I., Boyer, T. P., Garcia, H. E., Baranova, O. K., & Seidov, D. (2013). In S. Levitus, & A. V. Mishonov (Eds.), *World Ocean Atlas 2013 volume 1: Temperature*.
- McDougall, T. J. (1984). The relative roles of diapycnal and isopycnal mixing on subsurface water mass conversion. *Journal of Physical Oceanography*, 14(10), 1577–1589. [https://doi.org/10.1175/1520-0485\(1984\)014<1577:troda>2.0.co;2](https://doi.org/10.1175/1520-0485(1984)014<1577:troda>2.0.co;2)
- McDougall, T. J. (1987). Thermobaricity, cabbeling, and water-mass conversion. *Journal of Geophysical Research: Oceans*, 92(C5), 5448–5464. <https://doi.org/10.1029/jc092ic05p05448>
- McGillicuddy, D., Robinson, A., Siegel, D., Jannasch, H., Johnson, R., Dickey, T., et al. (1998). New evidence for the impact of mesoscale eddies on biogeochemical cycling in the Sargasso Sea. *Nature*, 394, 263–266. <https://doi.org/10.1038/28367>
- McGillicuddy, D., Jr, Anderson, L., Doney, S., & Maltrud, M. (2003). Eddy-driven sources and sinks of nutrients in the upper ocean: Results from a 0.1 resolution model of the North Atlantic. *Global Biogeochemical Cycles*, 17(2). <https://doi.org/10.1029/2002gb001987>
- McGillicuddy, D., Jr, & Robinson, A. (1997). Eddy-induced nutrient supply and new production in the Sargasso Sea. *Deep Sea Research Part I: Oceanographic Research Papers*, 44(8), 1427–1450. [https://doi.org/10.1016/s0967-0637\(97\)00024-1](https://doi.org/10.1016/s0967-0637(97)00024-1)
- Michaels, A. F., Knap, A. H., Dow, R. L., Gundersen, K., Johnson, R. J., Sorensen, J., et al. (1994). Seasonal patterns of ocean biogeochemistry at the US JGOFS Bermuda Atlantic Time-series Study site. *Deep Sea Research Part I: Oceanographic Research Papers*, 41(7), 1013–1038. [https://doi.org/10.1016/0967-0637\(94\)90016-7](https://doi.org/10.1016/0967-0637(94)90016-7)
- Naveira Garabato, A. C., Polzin, K. L., Ferrari, R., & Forryan, J. D. Z. A., (2016). A microscale view of mixing and overturning across the Antarctic Circumpolar Current. *Journal of Physical Oceanography*, 46, 233–254. <https://doi.org/10.1175/jpo-d-15-0025.1>
- Naveira Garabato, A. C., Ferrari, R., & Polzin, K. L. (2011). Eddy stirring in the Southern Ocean. *Journal of Geophysical Research: Oceans*, 116(C9). <https://doi.org/10.1029/2010jc006818>
- Nurser, A., Marsh, R., & Williams, R. G. (1999). Diagnosing water mass formation from air–sea fluxes and surface mixing. *Journal of Physical Oceanography*, 29(7), 1468–1487. [https://doi.org/10.1175/1520-0485\(1999\)029<1468:dwmffa>2.0.co;2](https://doi.org/10.1175/1520-0485(1999)029<1468:dwmffa>2.0.co;2)
- Oakey, N. S. (1982). Determination of the rate of dissipation of turbulent energy from simultaneous temperature and velocity shear microstructure measurements. *Journal of Physical Oceanography*, 12, 256–271. [https://doi.org/10.1175/1520-0485\(1982\)012<0256:dotrod>2.0.co;2](https://doi.org/10.1175/1520-0485(1982)012<0256:dotrod>2.0.co;2)
- Osborn, T. R. (1980). Estimates of the local rate of vertical diffusion from dissipation measurements. *Journal of Physical Oceanography*, 10, 83–89. [https://doi.org/10.1175/1520-0485\(1980\)010<0083:eotro>2.0.co;2](https://doi.org/10.1175/1520-0485(1980)010<0083:eotro>2.0.co;2)
- Oschlies, A. (2002). Can eddies make ocean deserts bloom? *Global Biogeochemical Cycles*, 16(4), 53–1. <https://doi.org/10.1029/2001gb001830>
- Redi, M. H. (1982). Oceanic isopycnal mixing by coordinate rotation. *Journal of Physical Oceanography*, 12(10), 1154–1158. [https://doi.org/10.1175/1520-0485\(1982\)012<1154:oimbcrc>2.0.co;2](https://doi.org/10.1175/1520-0485(1982)012<1154:oimbcrc>2.0.co;2)
- Resplandy, L., Lévy, M., Madec, G., Pous, S., Aumont, O., & Kumar, D. (2011). Contribution of mesoscale processes to nutrient budgets in the araban sea. *Journal of Geophysical Research: Oceans*, 116(C11). <https://doi.org/10.1029/2011jc007006>
- Roach, C. J., Balwada, D., & Speer, K. (2018). Global observations of horizontal mixing from argo float and surface drifter trajectories. *Journal of Geophysical Research: Oceans*, 123, 4560–4575. <https://doi.org/10.1029/2018jc013750>
- Stanley, R., Jenkins, W., Doney, S., & Lott, D. L., III (2015). The 3He flux gauge in the Sargasso Sea: A determination of physical nutrient fluxes to the euphotic zone at the Bermuda Atlantic Time-series Site. *Biogeosciences*, 12(17). <https://doi.org/10.5194/bg-12-5199-2015>
- Tennekes, H., & Lumley, J. L. (2018). *A first course in turbulence*. MIT press.
- Tuerena, R. & Mahaffey, C. (2021). Macromolar nutrient measurements from CTD niskin collected depth profiles in the Atlantic Ocean on cruise JR15007, June - July 2016 [Data set]. British Oceanographic Data Centre, National Oceanography Centre, NERC.
- Tuerena, R. E., Williams, R. G., Mahaffey, C., Vic, C., Green, J. A. M., Naveira-Garabato, A., & Sharples, J., (2019). Internal tides drive nutrient fluxes into the deep chlorophyll maximum over mid-ocean ridges. *Global Biogeochemical Cycles*, 33, 995–1009. <https://doi.org/10.1029/2019gb006214>
- Tulloch, R., Marshall, J., & Smith, K. S. (2009). Interpretation of the propagation of surface altimetric observations in terms of planetary waves and geostrophic turbulence. *Journal of Geophysical Research: Oceans*, 114, C02005. <https://doi.org/10.1029/2008jc005055>
- Uchida, T., Balwada, D., Abernathy, R. P., McKinley, G. A., Smith, S. K., & Lévy, M. (2020). Vertical eddy iron fluxes support primary production in the open Southern Ocean. *Nature Communications*, 11(1), 1–8. <https://doi.org/10.1038/s41467-020-14955-0>
- Vic, C., Garabato, A. C. N., Green, J. A. M., Spingys, C., Forryan, A., Zhao, Z., & Sharples, J. (2018). The lifecycle of semidiurnal internal tides over the northern mid-Atlantic ridge. *Journal of Physical Oceanography*, 48, 61–80. <https://doi.org/10.1175/jpo-d-17-0121.1>
- Waterhouse, A. F., MacKinnon, J. A., Nash, J. D., Alford, M. H., Kunze, E., Simmons, H. L., & Lee, C. M., (2014). Global patterns of diapycnal mixing from measurements of the turbulent dissipation rate. *Journal of Physical Oceanography*, 44, 1854–1872. <https://doi.org/10.1175/jpo-d-13-0104.1>
- Williams, R. G., & Follows, M. J. (1998). The Ekman transfer of nutrients and maintenance of new production over the North Atlantic. *Deep Sea Research Part I: Oceanographic Research Papers*, 45(2–3), 461–489. [https://doi.org/10.1016/s0967-0637\(97\)00094-0](https://doi.org/10.1016/s0967-0637(97)00094-0)
- Williams, R. G., & Follows, M. J. (2003). Physical transport of nutrients and the maintenance of biological production. In *Ocean biogeochemistry* (pp. 19–51). Springer. [https://doi.org/10.1007/978-3-642-55844-3\\_3](https://doi.org/10.1007/978-3-642-55844-3_3)
- Zika, J. D., & McDougall, T. J. (2008). Vertical and lateral mixing processes deduced from the mediterranean water signature in the North Atlantic. *Journal of Physical Oceanography*, 38, 164–176. <https://doi.org/10.1175/2007jpo3507.1>
- Zika, J. D., McDougall, T. J., & Sloyan, B. M. (2010). Weak mixing in the eastern North Atlantic: An application of the tracer-contour inverse method. *Journal of Physical Oceanography*, 40, 1881–1893. <https://doi.org/10.1175/2010jpo4360.1>
- Zweng, M. M., Reagan, J. R., Antonov, J. I., Locarnini, R. A., Mishonov, A. V., Boyer, T. P., & Biddle, M. M. (2013). In S. Levitus, & A. V. Mishonov (Eds.), *World Ocean Atlas 2013 volume 2: Salinity*.